

RCSTAT: A Statistical Framework for using Relative Contextualization in Transformers

Debabrata Mahapatra* Shubham Agarwal Apoorv Saxena Subrata Mitra
Adobe Research, India

Abstract

Prior work on input-token importance in auto-regressive transformers has relied on Softmax-normalized attention weights, which obscure the richer structure of pre-Softmax query-key logits. We introduce **RCSTAT**, a statistical framework that harnesses *raw attention logits* via *Relative Contextualization (RC)*—a random variable measuring contextual alignment between token segments—and derive an efficient upper bound for RC. We demonstrate two applications: (i) *Key-Value compression*, where RC-based thresholds drive adaptive key-value eviction for substantial cache reduction with minimal quality loss; and (ii) *Attribution*, where RC yields higher-fidelity token-, sentence-, and chunk-level explanations than post-Softmax methods. Across question answering, summarization, and attribution benchmarks, RCSTAT achieves significant empirical gains, delivering state-of-the-art compression and attribution performance without any model retraining.

1 Introduction

The transformer’s attention [51] mechanism encodes contextual relationships between tokens into internal state representations. This involves the raw dot-product similarity scores $\langle q, k \rangle$ of the query and key vectors, followed by a softmax normalization. Post-softmax attention weights are widely used for tasks such as attribution [56, 41] and memory optimization through Key-Value (KV) cache compression [21, 33, 34, 30]. However, such transformation introduces structural bias: it sharpens attention toward dominant tokens while flattening mid-range scores, thereby discarding subtle yet potentially meaningful contextual signals. Figure 1 visualizes pre-softmax attention logits ($\langle q, k \rangle$) from generated tokens to the prompt. Prompt tokens that are semantically relevant to the generation, i.e., carrying contextual alignment, consistently obtain higher logit values, while unrelated prompt tokens obtain lower logits. These meaningful differences are evident pre-softmax but are obscured post-softmax, where normalization flattens intermediate scores and skews attention [54] toward a few dominant or structurally favored positions (e.g., $\langle s \rangle$, $\langle /s \rangle$), referred to as *attention sink* phenomenon [24, 54].

Such information loss becomes consequential in applications requiring fine-grained relevance estimation use-cases, leading to inaccurate token attribution [29], sub-optimal KV-eviction [44], etc. While post-softmax weights represent localized attention at a specific layer, we posit that raw logits carry a dual role: they encode not only what the current layer attends to but also preserve upstream interactions, offering a richer statistical substrate for analysis.

Despite this potential, the usage of pre-softmax attention remains largely underexplored, primarily due to the lack of statistical tools and frameworks to extract structured insights from unnormalized logits. This work addresses that gap. We propose a probabilistic formalism that models relevance directly in the logit space, at different levels of granularity, enabling actionable and generalizable utilities across multiple downstream tasks.

*Corresponding Author, dmahapatra@adobe.com

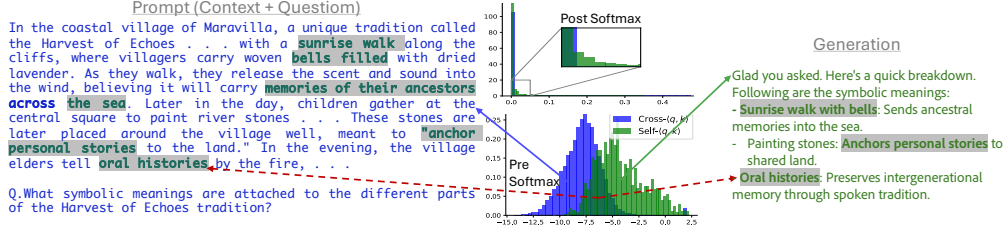


Figure 1: Attribution between generated text (right) and input prompt (left) is analyzed using pre-softmax attention logits vs. post-softmax values. The bottom histogram highlights pre-softmax logits, separating prompt tokens (cross- $\langle q, k \rangle$) from generated tokens (self- $\langle q, k \rangle$), at 13th layer 23th head from Llama-3B-instruct. Tokens in the overlapping region signify common content, a detail suppressed in the post-softmax histogram above. Using logit distributions, we can attribute (§ 4.2): (1) prompt parts not contextualized during generation (blue arrow), (2) generation parts uninfluenced by the prompt (green arrow), and (3) generation heavily contextualized by the prompt (red dashed arrows).

The informativeness of pre-softmax logits may not be the same across all attention heads. In fact, it is observed in literature that certain heads—often in the middle layers—demonstrate stronger contextual activity than others [41]. Recent interpretability efforts [16], such as circuit tracing [3], offer valuable but often qualitative insights into attention behavior. We take a complementary approach: quantifying how different attention heads behave and using that for grounding, attribution, and KV-cache compression. This enables task-driven analysis beyond hand-crafted patterns.

By operating in the logit space, our goal is to provide a principled and interpretable method for identifying such important heads, facilitating deeper insights into their functional roles. In other words, we propose a method for head-aware attention-logit analysis.

We summarize our contributions as follows:

1. We formalize the notion of contextualization as a set of random variables that capture the relationship between two portions of a text, e.g, a part of prompt and a part of generated tokens, within an attention head. Armed with these random variables, we introduce the relative contextualization (RC) to assign relevance scores at different levels of granularity, token-, chunk- and entire text level.
2. To estimate the statistics of RC, we derive a easy to compute practical intuitive upper bound and provide an efficient algorithm to compute it, which enables quantitative use of pre-softmax attention logits in downstream tasks.
3. In doing so, we propose RCSTAT, which to the best of our knowledge, is the first unified framework that brings different relevance assignment applications, such as KV-cache compression and token attribution, under one formalism.
4. We demonstrate with LLaMa models that RC-based KV-compression improves generation quality by 15–40% while achieving 2–5% higher compression than prior SOTA methods through adaptive head-wise eviction, and that RC-guided attribution—by selecting just 2% of attention heads—boosts token-, sentence-, and chunk-level accuracy by 2–3% on summarization, QA, and attribution benchmarks, all without any model retraining.

2 Related Work

Interpretability links generation outputs to the input and model internals. Compression and attribution translate this insight into action: the former prunes low-value signals; the latter assigns credit.

Mechanistic Interpretability of LLMs: Mechanistic interpretability [5] aims to reverse-engineer the internal workings of large language models. Circuit-tracing techniques [3, 18], such as those from Anthropic, have revealed neuron-level pathways and interpretable MLP circuits. Complementary efforts dissect self-attention heads [52], uncovering roles such as induction copying [37, 39] and positional tracking [15]. Beyond this, representation-level probes in BERT and GPT leverage attribution [42] and linear classifiers [14, 46, 8] to map hidden activations to semantic features. While

insightful, these methods often rely on heuristics [24] and remain largely qualitative. They lack a unified, quantitative framework and offer limited direct utility [58]. In contrast, our method analyzes the raw attention logits across heads via the statistical lens of Relative Contextualization (RC), to identify which heads are responsible for context-grounding and by how much.

KV Compression: KV cache can occupy up to 84% of inference memory for long contexts [26]. Prior reduction methods include quantization [26, 35, 31], low-rank approximation [7, 13], state merging [53, 2], and eviction [28]. We focus on eviction, discarding low-value key–value pairs. Eviction is classified into fixed-size and variable-size strategies. Fixed-size approaches enforce uniform budgets for every head and layer. Early methods, such as K-norm [12] and StreamingLLM [54], apply vector norm heuristics. Attention-based methods, such as SnapKV [30], TOVA [40] and H2O [57], rank tokens by post-softmax attention weights. QFilter [22] leverages linear algebra to isolate signal-carrying entries via matrix decompositions, and other methods in KVPress [27] use heuristics-based probabilistic scoring. Variable-size eviction strategies relax this by assigning heterogeneous budgets: PyramidKV [6] allocates caches to layers in a fixed pyramid schedule, whereas Ada-KV [20] refines this further by adjusting per-layer eviction budget based on estimated token relevance. However, manually fixing the cache budget risk degradation. In contrast, our method adaptively sets budgets per attention head via RC, yielding higher compression with minimal loss.

Attribution: Performing attribution is critical for trustworthy generation. Existing methods rely on either gradient signals or post-softmax attention weights. Gradient- and perturbation-driven methods such as Integrated Gradients [38, 49], LIME/SHAP [45, 36], and masking/occlusion [47] trace output sensitivity back to inputs but are computationally expensive. Attention-based methods aggregate post-softmax weights across heads and layers [1] or formulate attribution metrics [9]. However, averaging suppresses medium-strength token associations due to softmax normalization and the presence of sink tokens [41]. The learned explainer [11] mitigates this by assigning reliability scores to heads via a trained model on labeled data. In contrast, we use RC to assign per-head reliability scores without labeled data. Moreover, unlike the fixed offline weights used by the learned explainer, our per-example RC scores adapt on the fly, avoiding additional training overhead.

3 Self and Relative Contextualization in LM

To motivate our framework, we represent $\langle q, k \rangle$ as a random variable. This abstraction enables statistical reasoning in scenarios where decisions must be made at a chunk level rather than per token. For example, in KV-compression, eviction decisions must be made prior to generating an entire segment of text, not just individual tokens. Similarly, in attribution tasks, we aim to explain the influence of input tokens over contiguous output spans.

3.1 Probabilistic Formalism of Contextualization

Let V be the vocabulary of tokens and $\Omega \subset V^*$ be the sample space of all finite sequences of tokens. Let $(\Omega, 2^\Omega, P)$ be a probability space, where the probability measure $P(s)$ of a sequence $s = (t_1, t_2, \dots, t_n) \in \Omega$ is defined by an auto-regressive pre-trained transformer. For a given token sequence s , let the attention-logit be the function $f_s^{l,h} : [n] \times [n] \rightarrow \mathbb{R}$ that maps a pair of tokens at positions i and j to

$$f_s^{l,h}(i, j) = \begin{cases} \langle q_j^{l,h}, k_i^{l,h} \rangle & \text{for } i \leq j \leq n \\ -\infty & \text{otherwise,} \end{cases} \quad (1)$$

where $q_j^{l,h}$ and $k_i^{l,h}$ are the query and key vectors of h^{th} head in l^{th} layer. Our framework develops characteristics for individual heads, but we drop the superscript l,h for brevity henceforth.

A sequence has two parts, $s = p \oplus g$, where \oplus denotes concatenation, $p = \{t_1, \dots, t_m\}$ is the sequence of prompt tokens and $g = \{t_{m+1}, \dots, t_n\}$ is the sequence of generated tokens. The demarcation between p and g need not be rigidly associated with their names, prompt, and generation. The p could be a user-given prompt, a conversation history between the user and the language model, or a text that the language model is expected to continue. Similarly, g could be LLM-generated tokens or a portion of an existing text that needs to be analyzed with respect to its previous text p . If there is a user question between p and g , one may choose to place it at the end of p or the start of g .

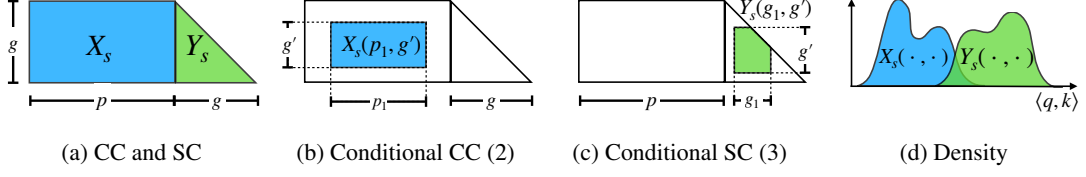


Figure 2: Illustration of the pre-softmax attention logits $Q^T K \in \mathbb{R}^{|s| \times |s|}$, where s is sequence s with prompt p and generated tokens g , as they appear in the last $|g|$ rows of the $Q^T K$ matrix. Figure 2a shows how the logits in the last $|g|$ rows are partitioned to construct the cross-contextualization (CC) and self-contextualization (SC) random variables. Figure 2b and 2c show the logits that construct conditional CC and conditional SC. Figure 2d shows their respective probability density function.

Next, we define four random variables, all illustrated in Figure 2, that capture the notion of contextualization at an attention-head level, a sequence level, and a sub-sequence level.

Definition 3.1 (Cross-Contextualization). We define cross-contextualization (CC) of an attention head in a transformer model as

$$F_X(X \leq x) := \sum_{s \in \Omega} P(s = p \oplus g) \sum_{t_i \in p} \sum_{t_j \in g} \frac{1}{|p||g|} \mathbf{1}(f_s(i, j) \leq x), \quad (\text{CC})$$

where $\mathbf{1}(\cdot)$ is the indicator function. The CC random variable captures the notion of contextualization between the prompt sequence and the generated sequence at a head-level. The same for a given sequence s can be formalized as a conditional RV $X|s$, whose CDF does not include the outermost summation of CC. The following definition further qualifies CC to a sub-sequence level.

Definition 3.2 (Conditional Cross-Contextualization). Assuming a sequence $s = p \oplus g$ with prompt tokens p and generated tokens g is given, and two subsets $p_1 \subset p$ and $g' \subset g$, whose complementary tokens $p \setminus p_1$ and $g \setminus g'$ are given, we define the conditional CC random variable $X_s(p_1, g')$ as

$$F_{X_s(p_1, g')}(X_s(p_1, g') \leq x) := F_X(X \leq x | s, p \setminus p_1, g \setminus g') = \sum_{t_i \in p_1} \sum_{t_j \in g'} \frac{\mathbf{1}(f_s(i, j) \leq x)}{|p_1||g'|}. \quad (2)$$

The conditional CC (2) represents the influence of prompt tokens in p_1 for generating tokens in g' . Note, if $p_1 = \{t_i\}$ and $g' = \{t_j\}$ are singleton sets, then the conditional CC $X_s(p_1, g')$ is simply a degenerate random variable at $x = f_s(i, j) = \langle q_j, k_i \rangle$. Similarly, if $p_1 = p$ and $g' = \{t_j\}$, the conditional CC corresponds to the values in $q_j^T K$, where $K \in \mathbb{R}^{d \times |p|}$ is the matrix of key vectors of prompt tokens. Trivially, $X_s(p, g) = X|s$.

Definition 3.3 (Self-Contextualization). We define self-contextualization (SC) of an attention head in a transformer model as

$$F_Y(Y \leq y) = \sum_{s \in \Omega} P(s = c \oplus g) \sum_{t_i, t_j \in g} \frac{2}{(|g| + 1)|g|} \mathbf{1}(i \leq j \wedge f_s(i, j) \leq y). \quad (\text{SC})$$

We define conditional SC similar to conditional CC in Definition 3.2.

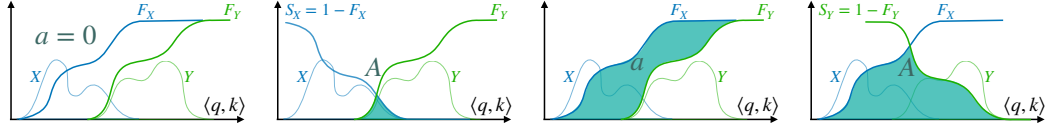
Definition 3.4 (Conditional Self-Contextualization). Assuming a sequence $s = p \oplus g$ is given, and two subsets of the generated tokens $g_1, g' \subset g$, whose complementary tokens $g \setminus g_1$ and $g \setminus g'$ are given, we define the conditional SC random variable $Y_s(g_1, g')$ as

$$F_{Y_s(g_1, g')}(Y_s(g_1, g') \leq y) := F_Y(Y \leq y | s, g \setminus g_1, g \setminus g') = \sum_{t_i \in g_1, t_j \in g'} \frac{\mathbf{1}(i \leq j \wedge f_s(i, j) \leq y)}{\sum_{t_i \in g_1, t_j \in g'} \mathbf{1}(i \leq j)}. \quad (3)$$

The conditional SC (3) represents the influences of tokens in g_1 for generating the tokens in g' that appear after g_1 . Trivially, $Y_s(g, g) = Y|s$.

3.2 Relative Contextualization

Due to the position embedding and auto-regressive nature of generation, in general, the self-contextualization values tend to be higher than those of cross-contextualization. However, some of the



(a) $a \leq \mathbb{E}[\max(X - Y, 0)]$ (b) $\mathbb{E}[\max(X - Y, 0)] \leq A$ (c) $a \leq \mathbb{E}[\max(Y - X, 0)]$ (d) $\mathbb{E}[\max(Y - X, 0)] \leq A$

Figure 3: Illustration of the upper and lower bounds stated in Theorem 3.6 for two types of relative contextualization: $\max(X - Y, 0)$ and $\max(Y - X, 0)$.

influential prompt tokens also receive higher softmax attention weights, suggesting that their $\langle q, k \rangle$ values must be higher than those of some of the generated tokens, since softmax is order-preserving. Formally, if $X_s(p_1, g) > Y_s(g_1, g)$ with high probability, then the (next-layer) value embeddings of the tokens in and after g_1 become heavily affected by the prompt tokens in p_1 . To measure the extent of this phenomenon, we introduce the notion of relative contextualization.

Definition 3.5 (Relative Contextualization). Assuming a sequence $s = p \oplus g$ is given, and two subsets $p_1 \subset p, g_1 \subset g$, whose complementary tokens $p \setminus p_1$ and $g \setminus g_1$ are given, we define the relative contextualization (RC) random variable as

$$Z_s(p_1, g_1) = \max(X_s(p_1, g) - Y_s(g_1, g), 0). \quad (\text{RC})$$

Similar to conditional CC and SC, $Z_s(p, g)$ is same as $Z|s = \max(X|s - Y|s, 0)$. Estimating the central statistics of RC requires an operation over the joint distribution of X and Y . If there are a large number of prompt and generated tokens, then computing any statistics of Z could become prohibitively expensive, as discussed in Section 3.3. Note, X_s and Y_s are not independent random variables since the key and query vectors of different tokens are intricately dependent on each other.

In the following, we derive a computationally efficient and practical upper bound for Eq. RC, without making any distributional assumptions on X_s or Y_s .

Theorem 3.6 (Area Under CDFs). *The expected relative contextualization Z is upper bounded by the overlap area A between, a) the area under the marginal CDF F_Y of self-contextualization Y , and b) the area under the marginal survival function S_X of cross-contextualization X :*

$$\mathbb{E}[Z_s(p_1, g_1)] \leq A_s(p_1, g_1) := \int_{-\infty}^{\infty} \min(F_{Y_s(g_1, g)}(t), S_{X_s(p_1, g)}(t)) dt, \quad (4)$$

where $S_X(t) = 1 - F_X(t)$, and lower bounded by the area a , under F_Y but over F_X :

$$a_s(p_1, g_1) := \int_{-\infty}^{\infty} \max(F_{Y_s(g_1, g)}(t) - F_{X_s(p_1, g)}(t), 0) dt \leq \mathbb{E}[Z_s(p_1, g_1)]. \quad (5)$$

Our proof of Theorem 3.6 in Appendix B is inspired by [4, 50] and uses copula [17]. Intuitively, the upper bound in (11) captures the area under the overlap region between the values of X and Y , as illustrated in Fig Figure 3b. The upper bound in (11) is tight for continuous CDFs F_X and F_Y (discussed in the proof). However, in our case, they are discrete. An alternative relative contextualization can be defined as $Z'_s(p_1, g_1) := \max(Y_s(g_1, g) - X_s(p_1, g), 0)$ that captures by how much the conditional SC is more than that of the conditional CC. The lower and upper bounds of Z'_s can be formulated similar to Z as in Theorem 3.6, and illustrated in Figure 3c and 3d.

3.3 Computational Complexity

We analyze the complexity of directly computing expected RC and computing its upper bound A_s (11) for all the prompt and generated tokens and a given attention head. For direct computation, if we make a simplifying assumption that the joint distribution of X_s and Y_s is a uniform distribution over its discrete support, the expected RC can be calculated as

$$\mathbb{E}[Z_s(p, g)] = \mathbb{E}[Z|s] = \frac{2}{|p||g|^2(|g| + 1)} \sum_{t_i \in p} \sum_{t_j = g} \sum_{t_k \in g} \sum_{t_l \in g: l \geq k} \max(f_s(i, j) - f_s(k, l), 0), \quad (6)$$

using $O(|p||g|^3)$ computations. Similarly, computation of $\mathbb{E}[Z_s(p_1, g_1)]$ requires $O(|p_1||g_1||g|^2)$ computations. An even simpler approximation is to use conditional expectation by assuming output

tokens are independent of each other and uniformly distributed: $\mathbb{E}[Z|s] \approx \mathbb{E}_{t_i \sim g}[\mathbb{E}[Z|s, \{t_i\}] = \mathbb{E}_{t_i \sim g}[\mathbb{E}[\max(X_s(p, \{t_j\}) - Y_s(g, \{t_j\}), 0)]]$. Although the complexity with this i.i.d. approximation is $O(|p||g|^2)$, which is less compared to that of (6), we observe that it performs poorly in downstream tasks such as KV-compression (see *Supplementary*). Hence, we do not use this approximation.

On the other hand, the upper bound A_s can be calculated in $\tilde{O}(|p||g| + |g|^2)$ computations, where $\tilde{O}(n) = O(n \log(n))$, with the Lebesgue integration approach in Algorithm 1. It involves sorting the samples of X_s and Y_s , individually in Line 1 and jointly in Line 2 to obtain the unique breakpoints B . With appropriate indexing, the complexity of computing CDFs and the minimum values in Lines 7, 8, and 9 becomes linear with respect to the number of midpoints M in Line 4. Similarly, the complexity of computing $A_s(p_1, g_1)$ is $\tilde{O}(|p_1||g| + |g_1||g|)$. Algorithm 1 can be easily extended to compute upper (11) and lower bound (12) for both types of RC in Figure 3 by modifying Line 9.

Algorithm 1 Area under $\min(F_{Y_s}, 1 - F_{X_s})$

Require: Samples of X_s and Y_s

Ensure: Overlap area A_s

```

1:  $X \leftarrow \text{sort}(X_s), Y \leftarrow \text{sort}(Y_s)$ 
2:  $B \leftarrow \text{unique}(\text{sort}(X \cup Y))$ 
3:  $L \leftarrow B_{1:\ell-1}, R \leftarrow B_{2:\ell} \quad \triangleright \ell = |B|$ 
4:  $M \leftarrow (L + R)/2 \quad \triangleright \text{Midpoints}$ 
5:  $W \leftarrow R - L \quad \triangleright \text{Widths}$ 
6: for each midpoint  $m_i \in M$  do
7:    $F_X(m_i) \leftarrow \frac{1}{n} \sum_j \mathbf{1}[X_j \leq m_i]$ 
8:    $F_Y(m_i) \leftarrow \frac{1}{m} \sum_j \mathbf{1}[Y_j \leq m_i]$ 
9:    $v_i \leftarrow \min(F_Y(m_i), 1 - F_X(m_i))$ 
10:  $A \leftarrow \sum_i v_i \cdot W_i \quad \triangleright \sim \text{Lebesgue Integral}$ 
11: return  $A$ 
```

Although the direct computation of RC in (6) becomes expensive when the number of generated tokens is high; it can be effective when $|g|$ is small. It offers the advantage of computing conditional RC for multiple parts of the prompt in parallel, which we leverage in the KV-compression task.

4 Applications of Relative Contextualization

Depending on the chosen subsets of the prompt and generated tokens, $p_1 \subset p$ and $g_1 \subset g$, Equation RC can support different applications. In this work, we explore two specific use cases.

4.1 KV Cache Compression

In an attention head, the value vector $v_j \in \mathbb{R}^d$ for a generated token t_j is computed, using the full KV-cache and under eviction, as:

$$v_j^* = \sum_{i \in [j]} \frac{e^{\langle q_j, k_i \rangle}}{\sum_{i \in [j]} e^{\langle q_j, k_i \rangle}} v_i, \quad \hat{v}_j = \sum_{i \in [j]: i \notin p_e} \frac{e^{\langle q_j, k_i \rangle}}{\sum_{i \in [j]: i \notin p_e} e^{\langle q_j, k_i \rangle}} v_i, \quad (7)$$

where $p_e \subset p$ denotes the set of prompt tokens whose key and value vectors are evicted. An ideal, but combinatorially hard to solve, eviction policy minimizes the degradation in value vector fidelity across all generated tokens g by finding an evictable token set p_e^* such that:

$$p_e^* = \underset{p_e \in 2^p}{\operatorname{argmin}} \frac{1}{|g|} \sum_{t_j \in g} \|v_j^* - \hat{v}_j\|_2. \quad (8)$$

However, g is unknown during decoding. Following SnapKV [30], we approximate g by using a window of the last few tokens in the prompt as a proxy \hat{g} . By treating expected RC as a score of significance, we decide whether to evict the KV of a token t_i , by comparing the scores for the singleton set $p_i = \{t_i\}$ with that of the entire prompt, i.e., evict if

$$\mathbb{E}[Z_p(p_i, \hat{g})] = \mathbb{E}[\max(X_p(p_i, \hat{g}) - Y_p(\hat{g}, \hat{g}))] \leq c \mathbb{E}[Z_p(p \setminus \hat{g}, \hat{g})], \quad (9)$$

where Z_p is defined similar to RC, but using the prompt p instead of the entire sequence s , and c is a compression hyperparameter. Eviction is adaptive: for a fixed c , each head selects a different p_e depending on its contextual load. We observe that a small-sized \hat{g} achieves better performance (see Section 5.2, hence, use (6) to compute the expected RC, instead of the upper bound (11)). We leave the exploration of other RC formulations in Figure 3 for score assignment as a future work.

4.2 Attribution to Context Tokens

Unlike KV-compression, the full token sequence $s = p \oplus g$ is known a priori in the attribution task. In general, the task is to find the spans in S that is most attributable to g' , given a generation token

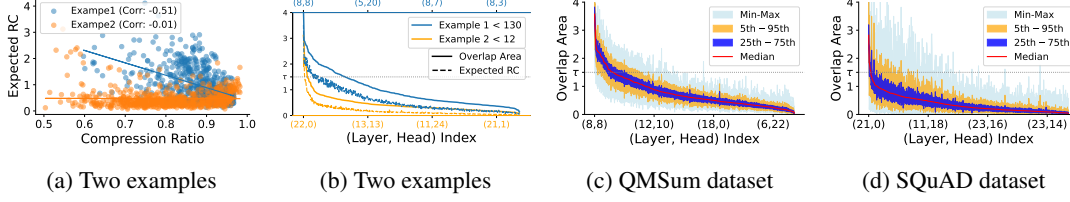


Figure 4: All plots are generated using the mentioned datasets with LLaMA-3B model: 28 layers, 24 heads in each layer. Figure 4b shows the sorted RC of the heads in the form of its expected value (6) and upper bound (11) (overlap area in Figure 3b). Figure 4c and 4d show the head-level overlap area across datasets, and the heads are sorted by their median overlap area. Figure 4a shows how the head-level compression ratio is anti-correlated with the RC score: each point corresponds to a head.

span $g' = [t_{j_1}, \dots, t_{j_2}]$ and a set of spans $S = \{p_1, \dots, p_{|S|}\}$ from the prompt. A prompt token span p_i could be: a chunk retrieved in the RAG setup, one of the few-shot examples for in-context learning, or a singleton token $p_i = \{t_i\}$ in the input prompt. Our attribution method has three steps.

Step 1: Compute the expected RC score $\mathbb{E}[Z_s^h]$ over the full token sequence s for each head h across all layers, then select the top- k heads \mathcal{H}_k .

Step 2: For each $p_i \in S$ and $h \in \mathcal{H}_k$, compute $\mathbb{E}[Z_s^h(p_i, g')]$, the expected RC from span p_i to generation span g' .

Step 3: Assign a normalized attribution score $\text{RC}(p_i)$ to each span $p_i \in S$ as:

$$\text{RC}(p_i) = \sum_{h \in \mathcal{H}_k} \frac{\mathbb{E}[Z_s^h(p_i, g')]}{\sum_{p_{i'} \in S} \sum_{h \in \mathcal{H}_k} \mathbb{E}[Z_s^h(p_{i'}, g')]} \quad (10)$$

Finally, we select the span p_i with the highest $\text{RC}(p_i)$. For long generations, we substitute the expected RC with its efficient upper bound (Eq. 11, visualized in Figure 3b) computed via Algorithm 1.

5 Experiments

We first study the behavior of RC by analyzing its expected scores and upper bounds across attention heads, and then evaluate its utility on two tasks: (i) KV-cache compression, and (ii) attribution. All experiments use LLaMA-3.2-3B and LLaMA-3.1-8B Instruct models [23].

Datasets: For analyzing attention heads and evaluating KV-cache compression, we use three benchmarks: 2000 examples from SQuAD v2.0 [43] (span-based QA with unanswerable queries), 200 from QMSum [59] (query-focused meeting summarization), and 2000 from 2WikiMultiHop [25] (multi-hop reading comprehension across linked Wikipedia articles). For evaluating attribution, we use 1300 examples from QuoteSum [48] (summaries annotated with source spans) and 200 from VERI-GRAN [41] (attribution in grounded generation). Please refer to Appendix A for more details.

5.1 Roles of Attention Heads Across Tasks

We analyze whether Relative Contextualization (RC) can distinguish relevant from irrelevant context, differentiate complex summarization from simple QA, and reveal how the number of contextualizing heads varies with the difficulty of the task.

Two Contrasting Examples: To illustrate, we use two prompts, each a context, question, and answer pair (Appendix C). We treat the context as the prompt and the concatenated question and answer as the generation. In Example 1, the context supports the question; in Example 2, it does not. Figure 4b shows that head-level RC scores, i.e., the relative contextualization (overlap) between prompt and generation, are uniformly lower for Example 2 with the irrelevant context across all heads and layers. This is reflected in the count of heads whose overlap upper bound exceeds a threshold $\tau = 1.5$; only 12 heads are responsible for contextualization for Example 2, compared to 130 heads for Example 1.

Sensitivity towards Task Complexity: Figure 4c shows that RC scores are substantially higher for QMSum (multi-sentence summarization) than for SQuAD (single-hop QA) in Figure 4d. On average, QMSum requires $9\times$ more high-RC-score heads than SQuAD ($p < 0.05$), indicating that complex tasks recruit a broader ensemble of attention heads, showing RC’s sensitivity to task difficulty.

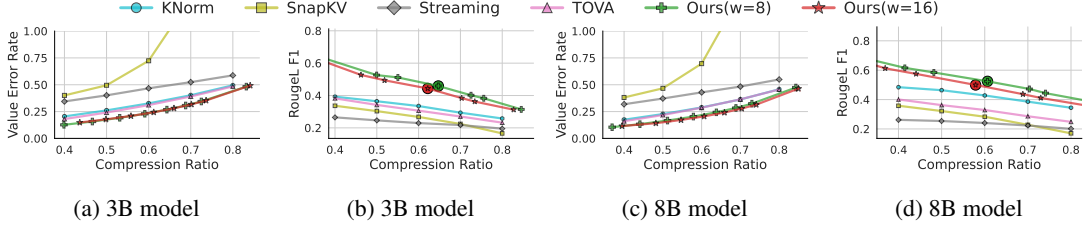


Figure 5: KV-cache compression performance on QMSum using LLaMA-3.2-3B and LLaMA-3.1-8B. We report Value Error Rate (VER \downarrow) and generation quality (RL-F1 \uparrow) across different strategies.

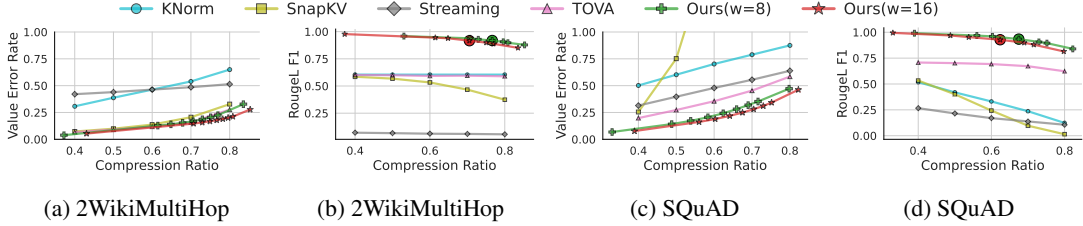


Figure 6: KV-cache compression results on 2WikiMultiHop and SQuAD v2.0 using LLaMA-3.1-8B.

Consistency of Heads Across Examples: Figures 4c and 4d also presents the distribution of overlap-area (min–max, 5th–95th, 25th–75th, median) for all 24×28 head-layer pairs on QMSum and SQuAD datasets respective, revealing a pronounced long-tail behavior: a handful of heads exhibit persistently large overlap across inputs, while most heads remain low. In the *Supplementary*, we provide detailed per-head distribution plots and heat maps for each dataset and model.

5.2 KV Cache Compression

Baselines: We compare our approach, RCSTAT, against state-of-the-art methods: Knorm [33], SnapKV [30], StreamingLLM [54], and TOVA [34]. Notably, both SnapKV and TOVA operate on post-softmax attention scores.

Metrics: The primary metric is compression ratio, the ratio between the number of evicted KV-caches and the total number of KV-caches across all layers and heads of the model. We evaluate the performance using ROUGE-1/L [32] and Value Error Rate (VER), the objective in Eq. (8) normalized by v_j^* inside the summation. For VER, we use the last layer’s value vectors of LLM and average across all heads and samples in the dataset. Unlike ROUGE, which measures textual overlap, VER captures how faithfully the model’s internal state is preserved under compression. We show some of our results in Figures 5 and 6, and all the results for 3 datasets and 2 LLaMA models in Appendix D.

Experimental Setup: We build upon the baseline implementations provided in the KVPress package [27], using default values for all method-specific hyperparameters. All baselines are evaluated at compression ratios of 0.4, 0.5, 0.6, 0.7, and 0.8. For RCSTAT, the compression ratio is controlled via the parameter c in (9), where larger values of c result in more aggressive eviction and thus higher compression. We vary c over 0.2, 0.7, 0.8, 1.0, 1.2, 1.3, 1.8, with the default setting $c=1$ highlighted using a circle in all plots. We also evaluate our method under different sliding window sizes for the last few tokens (see Section 4.1), with $w \in 8, 16$.

Generation-Compression Tradeoff: We show the results for VER metric in Figures 5a, 5c, 6a and 6c. Across all datasets and models, our method incurs the least VER for all compression ratios. These results show that the fidelity of the internal representation of generated tokens is best preserved in our method. Similarly, results in Figures 5b, 5d, 6b, and 6d, our method achieves the best solution frontier in the trade-off between compression ratio and RougeL F1 score. We notice that, although a lower VER implies higher RougeL, its inverse is not necessarily true: the ordering of solution frontiers of baselines for VER is not the same in RougeL-F1. This is expected, since RougeL measures n-gram output text overlap. In fact, even at 80 ~ 90% compression the an LLM generates answers, not from grounding in the context, but internal model weights learnt during pre-training [10, 19, 55].

Adaptive Head-wise Eviction: Our method adaptively determines the extent of KV-cache eviction at the level of individual attention heads. To analyze this behavior, we examine the correlation between

Table 1: Chunk-level accuracy for attributing extractive spans on QuoteSum and VERI-GRAN datasets (“HS” = Hidden States; “L3.1” = LLaMa-3.1).

Model	QuoteSum	VERI-GRAN
GPT-3.5 (inline)	90.18	26.40
GPT-4 (inline)	90.59	62.11
BM25	75.72	68.20
GTR	72.57	53.15
MT5	89.24	67.43
LLaMA-7B (HS [41])	87.51	77.33
Mistral-7B (HS [41])	89.95	77.71
L3.1-8B (all heads)	90.54	77.91
L3.1-8B (least RC, $k=20$)	29.49	2.81
L3.1-8B (most RC, $k=20$)	93.91	79.37

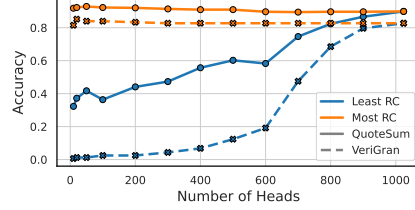


Figure 7: Attribution accuracy as we change number of attention heads, ranked by their RC scores

head-wise compression ratios and RC scores in Figure 4a, using the same examples as in Section 5.1. As anticipated, we observe a clear anti-correlation: heads with higher expected RC scores undergo less eviction, indicating their greater importance for context-grounded generation. For clarity, we report only means here; variances and other statistics appear in the *Supplementary*.

5.3 Attribution Detection

We enhance standard attention-based attribution [41] techniques by ranking heads via RC scores and retaining only the top- k heads. This focused selection yields consistent accuracy gains, whereas using the bottom- k heads injects noise from non-contextual heads (e.g., “attention-sink” heads) and drastically degrades performance.

Quantitative Results: On QuoteSum, selecting the top- k heads increases chunk-level accuracy by 3% over full-attention, while bottom- k selection incurs a 61% drop. On VERI-GRAN, top- k heads yield a 2% gain, whereas bottom- k heads fall to 2.8% (near random). Table 1 summarizes these results, confirming that RC isolates informative heads and filters out trivial ones.

Head-Selection Robustness: As noted above, we see a significant drop in performance when using the worst heads identified by RC. To dive deeper, Figure 7 shows attribution accuracy as a function of k . When using the top- k heads, accuracy remains near its peak even for small k . In contrast, accuracy plummets as more bottom- k heads are included, even up to 800 (out of 1024) heads. This demonstrates that RC enables selecting a compact, high-quality head subset without annotated attribution data, offering both accuracy improvements and potential compute savings.

The *Supplementary* includes: (i) qualitative examples of RC-guided improvements, and (ii) ablations showing that post-softmax attention scores cannot distinguish informative heads, unlike RC ranking.

6 Conclusion

We present RCSTAT, a statistical framework that computes Relative Contextualization (RC) from pre-softmax attention logits, and derive an efficient upper bound to enable practical applications in KV-cache compression and attribution without any model retraining. Empirically, RCSTAT sets a new state of the art in both tasks, demonstrating accuracy gains and potential compute savings.

Our analysis yields three key insights: (1) RC scores provide a principled metric for the contextualization effort required by an LLM, effectively quantifying task difficulty; (2) attention heads exhibit remarkably stable, example-agnostic contextualization patterns, revealing structured functional specialization; and (3) the most influential contextualization heads consistently reside in the model’s middle layers, corroborating prior findings.

Looking forward, the unexploited RC variants and logit-space bounds we proposed open avenues for robust hallucination detection, grounding evaluation, and dynamic context management. The framework also holds potential for assessing document coherence and enhancing explainable attribution. On the theoretical side, deriving probabilistic guarantees for RC-based compression quality is a compelling direction. Finally, scaling fine-grained, token-level RC for attribution, particularly in overlapping context regions, remains a challenging yet impactful problem for future work.

References

- [1] Samira Abnar and Willem Zuidema. Quantifying attention flow in transformers. *arXiv preprint arXiv:2005.00928*, 2020.
- [2] Shubham Agarwal, Sai Sundaresan, Subrata Mitra, Debabrata Mahapatra, Archit Gupta, Rounak Sharma, Nirmal Joshua Kapu, Tong Yu, and Shiv Saini. Cache-craft: Managing chunk-caches for efficient retrieval-augmented generation. *arXiv preprint arXiv:2502.15734*, 2025.
- [3] Emmanuel Ameisen, Jack Lindsey, Adam Pearce, Wes Gurnee, Nicholas L Turner, Brian Chen, Craig Citro, David Abrahams, Shan Carter, Basil Hosmer, et al. Circuit tracing: Revealing computational graphs in language models. *Transformer Circuits Thread*, 2025.
- [4] Marco De Angelis and Ander Gray. Why the 1-wasserstein distance is the area between the two marginal cdfs, 2021.
- [5] Anonymous. Mechanistic interpretability meets vision language models: Insights and challenges. *VLM Understanding Blog*, 2024.
- [6] Zefan Cai, Yichi Zhang, Bofei Gao, Yuliang Liu, Tianyu Liu, Keming Lu, Wayne Xiong, Yue Dong, Baobao Chang, Junjie Hu, et al. Pyramidkv: Dynamic kv cache compression based on pyramidal information funneling. *arXiv preprint arXiv:2406.02069*, 2024.
- [7] Chi-Chih Chang, Wei-Cheng Lin, Chien-Yu Lin, Chong-Yan Chen, Yu-Fang Hu, Pei-Shuo Wang, Ning-Chi Huang, Luis Ceze, Mohamed S Abdelfattah, and Kai-Chiang Wu. Palu: Compressing kv-cache with low-rank projection. *arXiv preprint arXiv:2407.21118*, 2024.
- [8] David Chanin, Anthony Hunter, and Oana-Maria Camburu. Identifying linear relational concepts in large language models. *arXiv preprint arXiv:2311.08968*, 2023.
- [9] Hila Chefer, Shir Gur, and Lior Wolf. Transformer interpretability beyond attention visualization. In *Proceedings of the IEEE/CVF conference on computer vision and pattern recognition*, pages 782–791, 2021.
- [10] Yung-Sung Chuang, Linlu Qiu, Cheng-Yu Hsieh, Ranjay Krishna, Yoon Kim, and James Glass. Lookback lens: Detecting and mitigating contextual hallucinations in large language models using only attention maps. *arXiv preprint arXiv:2407.07071*, 2024.
- [11] Benjamin Cohen-Wang, Yung-Sung Chuang, and Aleksander Madry. Learning to attribute with attention. *arXiv preprint arXiv:2504.13752*, 2025.
- [12] Alessio Devoto, Yu Zhao, Simone Scardapane, and Pasquale Minervini. A simple and effective l_2 norm-based strategy for kv cache compression. *arXiv preprint arXiv:2406.11430*, 2024.
- [13] Harry Dong, Xinyu Yang, Zhenyu Zhang, Zhangyang Wang, Yuejie Chi, and Beidi Chen. Get more with less: Synthesizing recurrence with kv cache compression for efficient llm inference. *arXiv preprint arXiv:2402.09398*, 2024.
- [14] Jason Du, Kelly Hong, Alishba Imran, Erfan Jahanparast, Mehdi Khfifi, and Kaichun Qiao. How gpt learns layer by layer. *arXiv preprint arXiv:2501.07108*, 2025.
- [15] Philipp Dufter, Martin Schmitt, and Hinrich Schütze. Position information in transformers: An overview. *Computational Linguistics*, 48(3):733–763, 2022.
- [16] Jacob Dunefsky, Philippe Chlenski, and Neel Nanda. Transcoders find interpretable llm feature circuits. *arXiv preprint arXiv:2406.11944*, 2024.
- [17] Fabrizio Durante and Carlo Sempì. Copula theory: An introduction. In Piotr Jaworski, Fabrizio Durante, Wolfgang Karl Härdle, and Tomasz Rychlik, editors, *Copula Theory and Its Applications*, pages 3–31, Berlin, Heidelberg, 2010. Springer Berlin Heidelberg.
- [18] Nelson Elhage, Catherine Olsson, Neel Nanda, et al. On the biology of a large language model, 2025. *Transformer Circuits*.

- [19] Philip Feldman, James R Foulds, and Shimei Pan. Trapping llm hallucinations using tagged context prompts. *arXiv preprint arXiv:2306.06085*, 2023.
- [20] Yuan Feng, Junlin Lv, Yukun Cao, Xike Xie, and S Kevin Zhou. Ada-kv: Optimizing kv cache eviction by adaptive budget allocation for efficient llm inference. *arXiv preprint arXiv:2407.11550*, 2024.
- [21] Suyu Ge, Yunan Zhang, Liyuan Liu, Minjia Zhang, Jiawei Han, and Jianfeng Gao. Model tells you what to discard: Adaptive kv cache compression for llms. In *The Twelfth International Conference on Learning Representations*.
- [22] Nathan Godey, Alessio Devoto, Yu Zhao, Simone Scardapane, Pasquale Minervini, Éric de la Clergerie, and Benoît Sagot. Q-filters: Leveraging qk geometry for efficient kv cache compression. *arXiv preprint arXiv:2503.02812*, 2025.
- [23] Aaron Grattafiori, Abhimanyu Dubey, Abhinav Jauhri, Abhinav Pandey, Abhishek Kadian, Ahmad Al-Dahle, Aiesha Letman, Akhil Mathur, Alan Schelten, Alex Vaughan, et al. The llama 3 herd of models. *arXiv preprint arXiv:2407.21783*, 2024.
- [24] Xiangming Gu, Tianyu Pang, Chao Du, Qian Liu, Fengzhuo Zhang, Cunxiao Du, Ye Wang, and Min Lin. When attention sink emerges in language models: An empirical view. *arXiv preprint arXiv:2410.10781*, 2024.
- [25] Xanh Ho, Anh-Khoa Duong Nguyen, Saku Sugawara, and Akiko Aizawa. Constructing a multi-hop QA dataset for comprehensive evaluation of reasoning steps. *International Committee on Computational Linguistics*.
- [26] Coleman Hooper, Sehoon Kim, Hiva Mohammadzadeh, Michael W Mahoney, Sophia Shao, Kurt Keutzer, and Amir Gholami. Kvquant: Towards 10 million context length llm inference with kv cache quantization. *Advances in Neural Information Processing Systems*, 37:1270–1303, 2024.
- [27] Simon Jegou, Maximilian Jeblick, and David Austin. kvpress. <https://github.com/NVIDIA/kvpress>, 2024. Version released 2024-11-13.
- [28] Haoyang Li, Yiming Li, Anxin Tian, Tianhao Tang, Zhanchao Xu, Xuejia Chen, Nicole Hu, Wei Dong, Qing Li, and Lei Chen. A survey on large language model acceleration based on kv cache management. *arXiv preprint arXiv:2412.19442*, 2024.
- [29] Yifei Li, Xiang Yue, Zeyi Liao, and Huan Sun. Attributionbench: How hard is automatic attribution evaluation?, 2024.
- [30] Yuhong Li, Yingbing Huang, Bowen Yang, Bharat Venkitesh, Acyr Locatelli, Hanchen Ye, Tianle Cai, Patrick Lewis, and Deming Chen. Snapkv: Llm knows what you are looking for before generation. *Advances in Neural Information Processing Systems*, 37:22947–22970, 2024.
- [31] Bokai Lin, Zihao Zeng, Zipeng Xiao, Siqi Kou, Tianqi Hou, Xiaofeng Gao, Hao Zhang, and Zhijie Deng. Matryoshkakv: Adaptive kv compression via trainable orthogonal projection. *arXiv preprint arXiv:2410.14731*, 2024.
- [32] Chin-Yew Lin. Rouge: A package for automatic evaluation of summaries. In *Text summarization branches out*, pages 74–81, 2004.
- [33] Akide Liu, Jing Liu, Zizheng Pan, Yefei He, Reza Haffari, and Bohan Zhuang. Minicache: Kv cache compression in depth dimension for large language models. *Advances in Neural Information Processing Systems*, 37:139997–140031, 2024.
- [34] Zichang Liu, Aditya Desai, Fangshuo Liao, Weitao Wang, Victor Xie, Zhaozhuo Xu, Anastasios Kyrillidis, and Anshumali Shrivastava. Scissorhands: Exploiting the persistence of importance hypothesis for llm kv cache compression at test time. *Advances in Neural Information Processing Systems*, 36:52342–52364, 2023.

- [35] Zirui Liu, Jiayi Yuan, Hongye Jin, Shaochen Zhong, Zhaozhuo Xu, Vladimir Braverman, Beidi Chen, and Xia Hu. Kivi: a tuning-free asymmetric 2bit quantization for kv cache. In *Proceedings of the 41st International Conference on Machine Learning*, pages 32332–32344, 2024.
- [36] Scott M Lundberg and Su-In Lee. A unified approach to interpreting model predictions. *Advances in neural information processing systems*, 30, 2017.
- [37] Callum McDougall, Arthur Conmy, Cody Rushing, Thomas McGrath, and Neel Nanda. Copy suppression: Comprehensively understanding an attention head. *arXiv preprint arXiv:2310.04625*, 2023.
- [38] Vivek Miglani, Aobo Yang, Aram H Markosyan, Diego Garcia-Olano, and Narine Kokhlikyan. Using captum to explain generative language models. *arXiv preprint arXiv:2312.05491*, 2023.
- [39] Catherine Olsson, Nelson Elhage, Neel Nanda, Nicholas Joseph, Nova DasSarma, Tom Henighan, Ben Mann, Amanda Askell, Yuntao Bai, Anna Chen, et al. In-context learning and induction heads. *arXiv preprint arXiv:2209.11895*, 2022.
- [40] Matanel Oren, Michael Hassid, Nir Yarden, Yossi Adi, and Roy Schwartz. Transformers are multi-state rnns. *arXiv preprint arXiv:2401.06104*, 2024.
- [41] Anirudh Phukan, Shwetha Somasundaram, Apoorv Saxena, Koustava Goswami, and Balaji Vasani Srinivasan. Peering into the mind of language models: An approach for attribution in contextual question answering. In *Findings of the Association for Computational Linguistics ACL 2024*, pages 11481–11495, 2024.
- [42] Maryam Rahimi, Yadollah Yaghoobzadeh, and Mohammad Reza Daliri. Explanations of deep language models explain language representations in the brain. *arXiv e-prints*, pages arXiv–2502, 2025.
- [43] Pranav Rajpurkar, Robin Jia, and Percy Liang. Know what you don’t know: Unanswerable questions for squad. *arXiv preprint arXiv:1806.03822*, 2018.
- [44] Siyu Ren and Kenny Q Zhu. On the efficacy of eviction policy for key-value constrained generative language model inference. *CoRR*, 2024.
- [45] Marco Tulio Ribeiro, Sameer Singh, and Carlos Guestrin. ” why should i trust you?” explaining the predictions of any classifier. In *Proceedings of the 22nd ACM SIGKDD international conference on knowledge discovery and data mining*, pages 1135–1144, 2016.
- [46] Anna Rogers, Olga Kovaleva, and Anna Rumshisky. A primer in bertology: What we know about how bert works. *Transactions of the association for computational linguistics*, 8:842–866, 2021.
- [47] David Schinagel, Georg Krispel, Horst Possegger, Peter M Roth, and Horst Bischof. Occam’s laser: Occlusion-based attribution maps for 3d object detectors on lidar data. In *Proceedings of the IEEE/CVF Conference on Computer Vision and Pattern Recognition*, pages 1141–1150, 2022.
- [48] Tal Schuster, Adam D Lelkes, Haitian Sun, Jai Gupta, Jonathan Berant, William W Cohen, and Donald Metzler. Semqa: Semi-extractive multi-source question answering. *arXiv preprint arXiv:2311.04886*, 2023.
- [49] Mukund Sundararajan, Ankur Taly, and Qiqi Yan. Axiomatic attribution for deep networks. In *International conference on machine learning*, pages 3319–3328. PMLR, 2017.
- [50] S. S. Vallender. Calculation of the wasserstein distance between probability distributions on the line. *Theory of Probability & Its Applications*, 18(4):784–786, 1974.
- [51] Ashish Vaswani, Noam Shazeer, Niki Parmar, Jakob Uszkoreit, Llion Jones, Aidan N. Gomez, Łukasz Kaiser, and Illia Polosukhin. Attention is all you need. In *Proceedings of the 31st International Conference on Neural Information Processing Systems, NIPS’17*.

- [52] Elena Voita, David Talbot, Fedor Moiseev, Rico Sennrich, and Ivan Titov. Analyzing multi-head self-attention: Specialized heads do the heavy lifting, the rest can be pruned. *arXiv preprint arXiv:1905.09418*, 2019.
- [53] Zheng Wang, Boxiao Jin, Zhongzhi Yu, and Minjia Zhang. Model tells you where to merge: Adaptive kv cache merging for llms on long-context tasks. *arXiv preprint arXiv:2407.08454*, 2024.
- [54] Guangxuan Xiao, Yuandong Tian, Beidi Chen, Song Han, and Mike Lewis. Efficient streaming language models with attention sinks. *arXiv preprint arXiv:2309.17453*, 2023.
- [55] Ziwei Xu, Sanjay Jain, and Mohan Kankanhalli. Hallucination is inevitable: An innate limitation of large language models. *arXiv preprint arXiv:2401.11817*, 2024.
- [56] Xiang Yue, Boshi Wang, Ziru Chen, Kai Zhang, Yu Su, and Huan Sun. Automatic evaluation of attribution by large language models. In *Findings of the Association for Computational Linguistics: EMNLP 2023*, pages 4615–4635, 2023.
- [57] Zhenyu Zhang, Ying Sheng, Tianyi Zhou, Tianlong Chen, Lianmin Zheng, Ruisi Cai, Zhao Song, Yuandong Tian, Christopher Ré, Clark Barrett, et al. H2o: Heavy-hitter oracle for efficient generative inference of large language models. *Advances in Neural Information Processing Systems*, 36:34661–34710, 2023.
- [58] Haiyan Zhao, Hanjie Chen, Fan Yang, Ninghao Liu, Huiqi Deng, Hengyi Cai, Shuaiqiang Wang, Dawei Yin, and Mengnan Du. Explainability for large language models: A survey. *ACM Transactions on Intelligent Systems and Technology*, 15(2):1–38, 2024.
- [59] Ming Zhong, Da Yin, Tao Yu, Ahmad Zaidi, Mutethia Mutuma, Rahul Jha, Ahmed Hassan Awadallah, Asli Celikyilmaz, Yang Liu, Xipeng Qiu, and Dragomir Radev. QMSum: A new benchmark for query-based multi-domain meeting summarization. Association for Computational Linguistics.

A Appendix: Reproducibility Details

Code and Assets. We use publicly available code, models, and datasets, cited and listed below with corresponding licenses and versions.

- **Codebase:** We build upon [KVPress] <https://github.com/NVIDIA/kvpress>. *Version:* 3dbf8f4 *License:* Apache 2.0
- **Models:** We use LLaMA Model from [23]. *URL:* <https://huggingface.co/meta-llama/Llama-3.2-3B-Instruct> *URL:* <https://huggingface.co/meta-llama/Llama-3.1-8B-Instruct> *License:* Llama 3.1 and Llama 3.2 Community License
- **Datasets:** We use datasets as follows:
 - **QMSum** [59] *Version:* Latest GitHub release (accessed 2025-05) *URL:* <https://github.com/Yale-LILY/QMSum> *License:* MIT License
 - **2WikiMultihopQA** [25] *Version:* Latest GitHub release (accessed 2025-05) *URL:* <https://github.com/Alab-NII/2wikimultihop> *License:* Apache 2.0
 - **SQuAD v2.0** [43] *Version:* Hugging Face release (accessed 2025-05) *URL:* https://huggingface.co/datasets/rajpurkar/squad_v2 *License:* CC BY-SA 4.0
 - **QuoteSum** [48] *Version:* GitHub release (accessed 2025-05) *URL:* <https://github.com/google-research-datasets/QuoteSum> *License:* CC BY-SA 4.0
 - **Verifiability-Granular** [41] *Version:* GitHub release (accessed 2025-05) *URL:* <https://github.com/Anirudh-Phukan/verifiability-granular> *License:* CC BY-SA 4.0

Environment. Experiments were conducted using PyTorch 2.1, CUDA 12.1 on A100 80GB, with code and instructions to be made available.

B Appendix: Theoretical Results

Theorem 3.6 (Area Under CDFs). *The expected relative contextualization Z is upper bounded by the overlap area A between, a) the area under the marginal CDF F_Y of self-contextualization Y , and b) the area under the marginal survival function S_X of cross-contextualization X :*

$$\mathbb{E}[Z_s(p_1, g_1)] \leq A_s(p_1, g_1) := \int_{-\infty}^{\infty} \min(F_{Y_s(g_1, g)}(t), S_{X_s(p_1, g)}(t)) dt, \quad (11)$$

where $S_X(t) = 1 - F_X(t)$, and lower bounded by the area a , under F_Y but over F_X :

$$a_s(p_1, g_1) := \int_{-\infty}^{\infty} \max(F_{Y_s(g_1, g)}(t) - F_{X_s(p_1, g)}(t), 0) dt \leq \mathbb{E}[Z_s(p_1, g_1)]. \quad (12)$$

Proof. Following [50], $\kappa = \mathbb{E}[\max(X - Y, 0)]$ can be written as

$$\kappa = \int_{-\infty}^{\infty} P(X > t \text{ and } Y \leq t) dt \quad (13)$$

$$= \int_{-\infty}^{\infty} (P(Y \leq t) - P(X \leq t \text{ and } Y \leq t)) dt. \quad (14)$$

Applying Sklar’s theorem [17], the joint CDF $P(X \leq t \text{ and } Y \leq t)$ can be written as a copula C distribution of marginal CDF values:

$$\kappa = \int_{-\infty}^{\infty} (F_Y(t) - C(F_X(t), F_Y(t))) dt. \quad (15)$$

Let $u = F_X(t)$ and $v = F_Y(t)$. Applying Fréchet–Hoeffding bound [17],

$$\max(u + v - 1, 0) \leq C(u, v) \leq \min(u, v) \quad (16)$$

$$\Rightarrow v - \min(u, v) \leq v - C(u, v) \leq v - \max(u + v - 1, 0) \quad (17)$$

$$\Rightarrow v - (\min(u - v, 0) + v) \leq v - C(u, v) \leq v - (\max(u - 1, -v) + v) \quad (18)$$

$$\Rightarrow \max(v - u, 0) \leq v - C(u, v) \leq \min(1 - u, v). \quad (19)$$

We complete the proof by integrating all sides of (19) w.r.t. t . \square

Note, since our CDFs are for discrete random variable, F_X and F_Y are not continuous. Therefore, Sklar's theorem doesn't guarantee a unique copula C for the $P(X \leq t \text{ and } Y \leq t)$. Moreover, since joint distribution will also be discrete, it will not be invertible. Therefore, we cannot guarantee that the upper bound in Fréchet–Hoeffding bound to be tight.

Corollary B.1. *For any small $\delta > 0$, the relative contextualization is upper bounded as*

$$Z_s(p_1, g_1) \leq \frac{A_s(p_1, g_1)}{\delta} \quad (20)$$

with probability at least $1 - \delta$.

Proof. Let $Z := Z_s(p_1, g_1)$ and $A := A_s(p_1, g_1)$. From Theorem 3.6 we know that $\mathbb{E}[Z] \leq A$.

Now, by Markov's inequality, for any $\delta > 0$, we have:

$$\Pr\left(Z \geq \frac{A}{\delta}\right) \leq \frac{\mathbb{E}[Z]}{A/\delta} \leq \frac{A}{A/\delta} = \delta.$$

Therefore, with probability at least $1 - \delta$, we have:

$$Z < \frac{A}{\delta}.$$

Hence,

$$Z_s(p_1, g_1) \leq \frac{A_s(p_1, g_1)}{\delta}$$

with probability at least $1 - \delta$, as claimed. \square

C Appendix: Two contrasting examples

<p>In the coastal village of Maravilla, a unique tradition called the Harvest of Echoes takes place every October. The event, though relatively unknown outside the region, holds deep cultural meaning for the villagers. The tradition begins with a sunrise walk along the cliffs, where villagers carry woven bells filled with dried lavender. As they walk, they release the scent and sound into the wind, believing it will carry memories of their ancestors across the sea. Later in the day, children gather at the central square to paint river stones with symbols from their family histories. These stones are later placed around the village well, meant to "anchor personal stories to the land." In the evening, the village elders tell oral histories by the fire, including tales of migration, war, lost siblings, and recovered friendships. These stories are not written down but are expected to be retold from memory by the youth in coming years, emphasizing the importance of intergenerational memory. Visitors are welcomed to observe, but only those born in Maravilla may participate fully. The community believes that participation requires a personal connection to the land, the well, and the stories passed down.</p> <p>Q: What symbolic meanings are attached to the different parts of the Harvest of Echoes tradition?</p> <p>G: Following are the symbolic meanings:</p> <ul style="list-style-type: none"> • Sunrise walk with bells: Sends ancestral memories into the sea. • Painting stones: Anchors personal stories to shared land. • Oral histories: Preserves intergenerational memory through spoken tradition.
--

Figure 8: Example 1: Relevant context

In the modern software development landscape, programming languages serve as essential tools that enable developers to create everything from simple scripts to complex systems and applications. Over the years, several programming languages have gained significant popularity due to their versatility, ease of use, performance, and applicability across different domains. Understanding the characteristics and use cases of these languages provides a strong foundation for anyone entering the field of computer science or software engineering.

Below is a detailed overview of some of the most popular and widely-used programming languages in the industry today:

Python: Python is a high-level, interpreted programming language renowned for its simplicity and readability, which makes it particularly appealing to beginners. Its clear and concise syntax mimics natural language, allowing developers to write logical code with fewer lines. Python supports multiple programming paradigms, including procedural, object-oriented, and functional programming. One of its key strengths lies in its vast ecosystem of libraries and frameworks, which extend its functionality into areas such as web development (e.g., Django, Flask), data analysis (e.g., Pandas, NumPy), machine learning and artificial intelligence (e.g., TensorFlow, PyTorch), and automation. Its platform independence and active community support have contributed to its rapid rise in popularity, making it one of the most in-demand languages across both academia and industry.

JavaScript: JavaScript is a dynamic, high-level scripting language primarily used for client-side web development. Originally developed to enhance interactivity in web browsers, JavaScript has evolved into a powerful and versatile language capable of running on both the client and server sides. Through modern frameworks and libraries such as React, Angular, and Vue.js, JavaScript enables developers to build rich, responsive user interfaces. On the backend, JavaScript is widely used with environments like Node.js, which allow it to be used for server-side programming. The language supports event-driven programming and asynchronous processing, making it ideal for developing web applications that require real-time interaction, such as chat applications and collaborative tools. Its ubiquity across the web and ease of integration with HTML and CSS make JavaScript an indispensable tool in the modern web development stack.

Java: Java is a statically-typed, object-oriented programming language that is known for its portability, stability, and scalability. It follows the principle of "write once, run anywhere," meaning compiled Java code can run on any platform that supports the Java Virtual Machine (JVM). Java is a go-to language for building enterprise-level applications, including financial systems, enterprise resource planning (ERP) software, and large-scale web services. Additionally, Java is the primary language used for developing Android applications, making it a cornerstone in the mobile app development ecosystem. Its strong memory management, robust security features, and extensive standard libraries make Java suitable for high-performance applications and distributed systems. Java's long-standing presence in academia and the corporate world continues to ensure its relevance in modern software development.

C++: C++ is a powerful, high-performance programming language that extends the C programming language with object-oriented features. It is widely regarded for its fine-grained control over system resources and hardware, which makes it ideal for developing performance-critical applications. C++ is commonly used in system/software development, including operating systems, embedded systems, and real-time systems. It is also prevalent in the game development industry, where low-level memory manipulation and high-speed performance are crucial. Furthermore, C++ is popular in competitive programming and algorithmic challenges due to its speed and flexibility. The language supports both procedural and object-oriented programming paradigms and includes features such as classes, templates, exception handling, and the Standard Template Library (STL), which provides useful data structures and algorithms. While it has a steeper learning curve than some other languages, C++ remains a fundamental language for understanding core computer science concepts and software design.

In conclusion, these languages—Python, JavaScript, Java, and C++—each offer unique strengths and are suited to different domains and project requirements. Their widespread use and strong community support make them essential tools in the toolkit of any developer.

Q: How to terraform Mars?

G: I think there may be a bit of a problem here! Terraforming Mars is a hypothetical process of making the planet habitable for humans and other Earth-like species. While it's an intriguing concept, it's still largely in the realm of science fiction... for now. Currently, there is no known method or technology that can terraform Mars, and it's unlikely that we'll see significant progress in this area soon. The challenges involved are enormous, including:

1. Distance and communication: Mars is about 140 million miles away from Earth, making it difficult to send resources and personnel.
2. Harsh environment: Mars has a thin atmosphere, extreme temperatures, and toxic chemicals that make it inhospitable to human life.
3. Radiation: Mars lacks a strong magnetic field, which means that radiation from the sun and deep space can be harmful to humans.
4. Gravity: Mars' gravity is only about one-third of Earth's, which can cause a range of health problems for humans.

While there are some concepts and proposals for terraforming Mars, they are still largely theoretical and require significant scientific and technological advancements before they can be considered feasible.

Figure 9: Example 2: Irrelevant context

D Appendix: Plots

This appendix presents all evaluation plots across datasets (QMSum, 2WikiMultiHop, SQuAD) and model sizes (3B, 8B). Each plot compares performance metrics—VER, ROUGE-1 F1, and ROUGE-L F1—across different configurations. A shared legend is included for clarity, and plots are grouped by metric and model size for visual consistency.

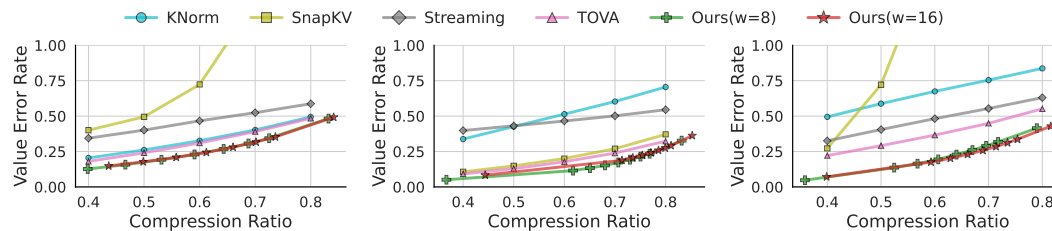


Figure 10: VER scores for 3B model on QMSum, 2WikiMultiHop, and SQuAD datasets.

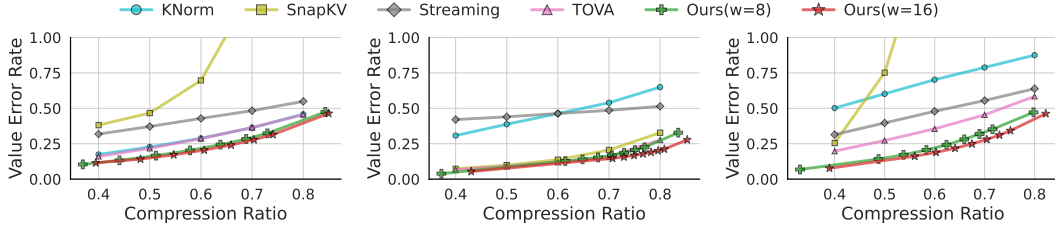


Figure 11: VER scores for 8B model on QMSum, 2WikiMultiHop, and SQuAD datasets.

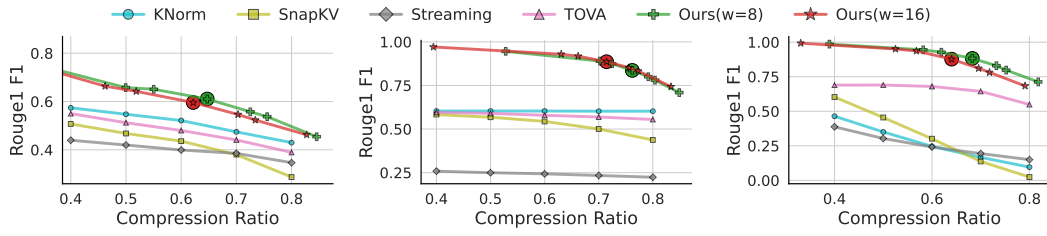


Figure 12: ROUGE-1 F1 scores for 3B model on QMSum, 2WikiMultiHop, and SQuAD datasets.

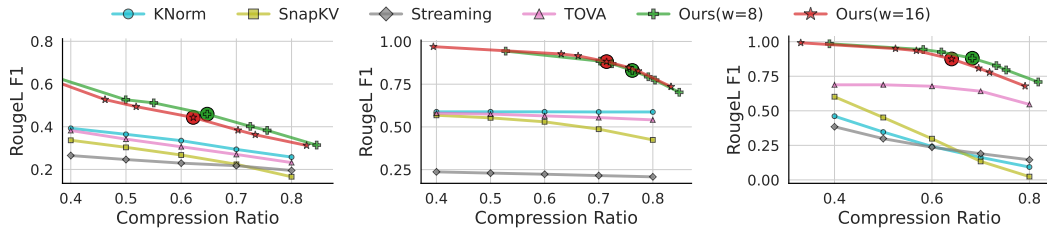


Figure 13: ROUGE-L F1 scores for 3B model on QMSum, 2WikiMultiHop, and SQuAD datasets.

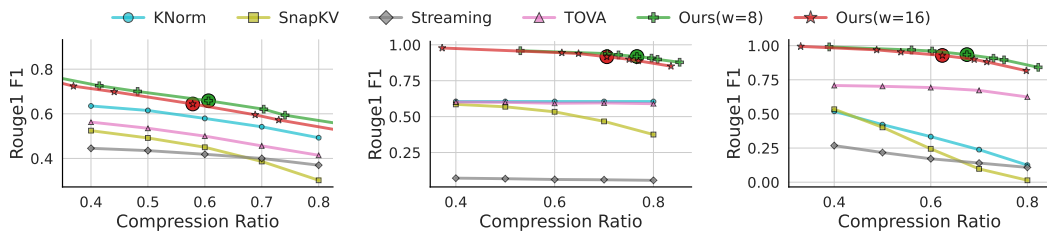


Figure 14: ROUGE-1 F1 scores for 8B model on QMSum, 2WikiMultiHop, and SQuAD datasets.

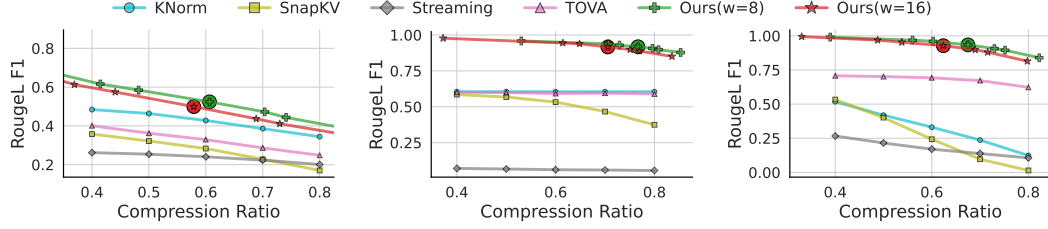


Figure 15: ROUGE-L F1 scores for 8B model on QMSum, 2WikiMultiHop, and SQuAD datasets.

E Appendix: Preliminaries

Let $X = [x_1, x_2, \dots, x_T] \in \mathbb{R}^{T \times d}$ be the input sequence of length T , where each $x_i \in \mathbb{R}^d$ is an input token embedding and d is the model’s hidden dimension. For each attention head $h \in \{1, \dots, H\}$ in layer $\ell \in \{1, \dots, L\}$, define

$$Q^{(\ell,h)} = XW_Q^{(\ell,h)}, \quad K^{(\ell,h)} = XW_K^{(\ell,h)}, \quad V^{(\ell,h)} = XW_V^{(\ell,h)}, \quad (21)$$

where $Q^{(\ell,h)}, K^{(\ell,h)}, V^{(\ell,h)} \in \mathbb{R}^{T \times d_h}$ and $d_h = d/H$.

Attention Logits. The pre-softmax attention logits are given by

$$Z^{(\ell,h)} = Q^{(\ell,h)}(K^{(\ell,h)})^\top \in \mathbb{R}^{T \times T}, \quad z_{i,j}^{(\ell,h)} = \langle q_i^{(\ell,h)}, k_j^{(\ell,h)} \rangle. \quad (22)$$

Attention Weights. The post-softmax weights are

$$A^{(\ell,h)} = \text{softmax}\left(\frac{Z^{(\ell,h)}}{\sqrt{d_h}}\right), \quad a_{i,j}^{(\ell,h)} = \frac{\exp(z_{i,j}^{(\ell,h)}/\sqrt{d_h})}{\sum_{j'} \exp(z_{i,j'}^{(\ell,h)}/\sqrt{d_h})}. \quad (23)$$

Attention Output. The output of the head is

$$Y^{(\ell,h)} = A^{(\ell,h)}V^{(\ell,h)} \in \mathbb{R}^{T \times d_h}, \quad (24)$$

and the full multi-head output is

$$\text{MHA}^{(\ell)}(X) = \left[Y^{(\ell,1)} \parallel \dots \parallel Y^{(\ell,H)} \right] W_O^{(\ell)} \in \mathbb{R}^{T \times d}. \quad (25)$$

We refer to $Z^{(\ell,h)}$ and $A^{(\ell,h)}$ as the pre-softmax affinities and post-softmax attention weights, respectively. While $A^{(\ell,h)}$ normalizes attention for token interaction, it also suppresses informative patterns in $Z^{(\ell,h)}$. Our work leverages Z directly to extract statistical signals useful for contextual analysis, KV compression, and attribution.

Table 2: **Value Error Rate (VER)** on the QMSum dataset across different compression ratios (50%, 60%, 70%) for LLaMA-3.2-3B and LLaMA-3.1-8B Instruct models. **RCStat (IOT)** assumes *Independent Output Tokens*, while **RCStat (Non-IOT)** does not assume any independence. Here, lower is better.

Model	Method	50%	60%	70%
3B	TOVA	0.2408	0.3103	0.3905
	RCSTAT (IOT)	0.1956	0.2648	0.3402
	RCSTAT (Non-IID)	0.1571	0.2295	0.3066
8B	TOVA	0.2177	0.2859	0.3639
	RCSTAT (IOT)	0.1615	0.2290	0.3007
	RCSTAT (Non-IID)	0.1043	0.2034	0.2836

F Relative Contextualization distribution: Head-level Analysis

We show the per-head distribution of relative contextualization, in terms of the upper bound overlap area, in Figures 16, 17, and 18 for QMSum, Squadv2, and 2WikiMultiHop datasets, respectively. The percentile values of these distributions are shown in Figures 19, 20, and 21 respectively. These figures provide empirical evidence of our statement in the conclusion section: “the most influential contextualization heads consistently reside in the model’s middle layers, corroborating prior findings.” This can also be observed in Figures 4c and 4d in the main paper, where the high-scoring heads correspond to the middle layers: layer indices are shown in the x-axis labels.

G Complete Experimental Statistics for KV-compression results

Please find the results of Value Error Rate (VER) inside the VER folder. For the baseline methods, the mean and standard deviations of VER for different compression ratios are saved in csv files with the naming format <dataset>_<model>_baseline_df.csv, where the dataset field can be 2WikiMultiHop, QMSum, or SQuAD, and the model field can be 3b or 8b. Similarly, the mean and standard deviations of VER and the mean and standard deviations of the compression ratios for different threshold multipliers are saved in csv files with the naming format <dataset>_<model>_proposed_df.csv. Similarly, the results for Rouge1 and RougeL can be found in the All_Rouges folder.

G.1 Independence assumption of generated tokens

The result in Table 2 shows that the fidelity of value vectors is higher when RCSTAT is executed without assuming independence for the random variables corresponding to $\langle q, k \rangle$ of generated tokens. Nonetheless, even with the independence assumption, RCSTAT outperforms TOVA, which is the best-performing method in our experiments for the main paper.

H Additional Results for Attribution Experiments

H.1 Qualitative Comparison of Attribution Strategies at Layer 15

To better understand the effectiveness of various attention-based attribution strategies, we compare three different approaches using attention maps from Layer 15 of our model: (1) the mean attention across all heads, (2) the top-scoring head according to our attribution scoring technique, and (3) the worst-scoring head by the same measure. All methods were evaluated on the same input setup: a sales report document with the question “What were the product sales on November 21st?” and the answer “The product sales on November 21st were \$177.00.”

Figure 22 presents the attention heatmaps produced by each of the three strategies. The top-scoring head (Head 30, Figure 22a) yields a sharply focused attribution map, precisely attending to tokens corresponding to the correct numerical value. In contrast, the mean attention across all heads (Figure 22b) produces a reasonable heatmap but also attends to several unrelated tokens, leading to

Table 3: Additional result for the attribution task, when head selection is based on Relative contextualization applied on post-softmax.

Model	QuoteSum	VERI-GRAN
GPT-3.5 (inline)	90.18	26.40
GPT-4 (inline)	90.59	62.11
BM25	75.72	68.20
GTR	72.57	53.15
MT5	89.24	67.43
LLaMA-7B (HS)	87.51	77.33
Mistral-7B (HS)	89.95	77.71
L3.1-8B (all heads)	90.54	77.91
L3.1-8B (least RC post-softmax, $k=20$)	35.72	4.69
L3.1-8B (least RC pre-softmax, $k=20$)	29.49	2.81
L3.1-8B (most RC post-softmax, $k=20$)	90.03	71.25
L3.1-8B (most RC pre-softmax, $k=20$)	93.91	79.37

less interpretable attributions. Finally, the worst-scoring head (Head 16, Figure 22c) demonstrates diffuse and uninformative attention, highlighting mostly irrelevant tokens.

These observations qualitatively validate our scoring technique for identifying high-quality attribution heads and demonstrate that selectively using the best attention heads can significantly improve interpretability.

H.2 Quantitative Comparison for Post-softmax and pre-softmax

In Table 3 we present the quantitative result of what happens if the head selection is based on the RC applied to post-softmax attention weights instead of pre-softmax attention logits. We observe that, when top heads are based on post-softmax weights, the attribution accuracy is lower than that of pre-softmax, whereas when the bottom heads are based on post-softmax weights, the attribution accuracy is not lower compared to pre-softmax. This shows that the information that can distinguish head-level importance is present more in pre-softmax logit values than in post-softmax weights.

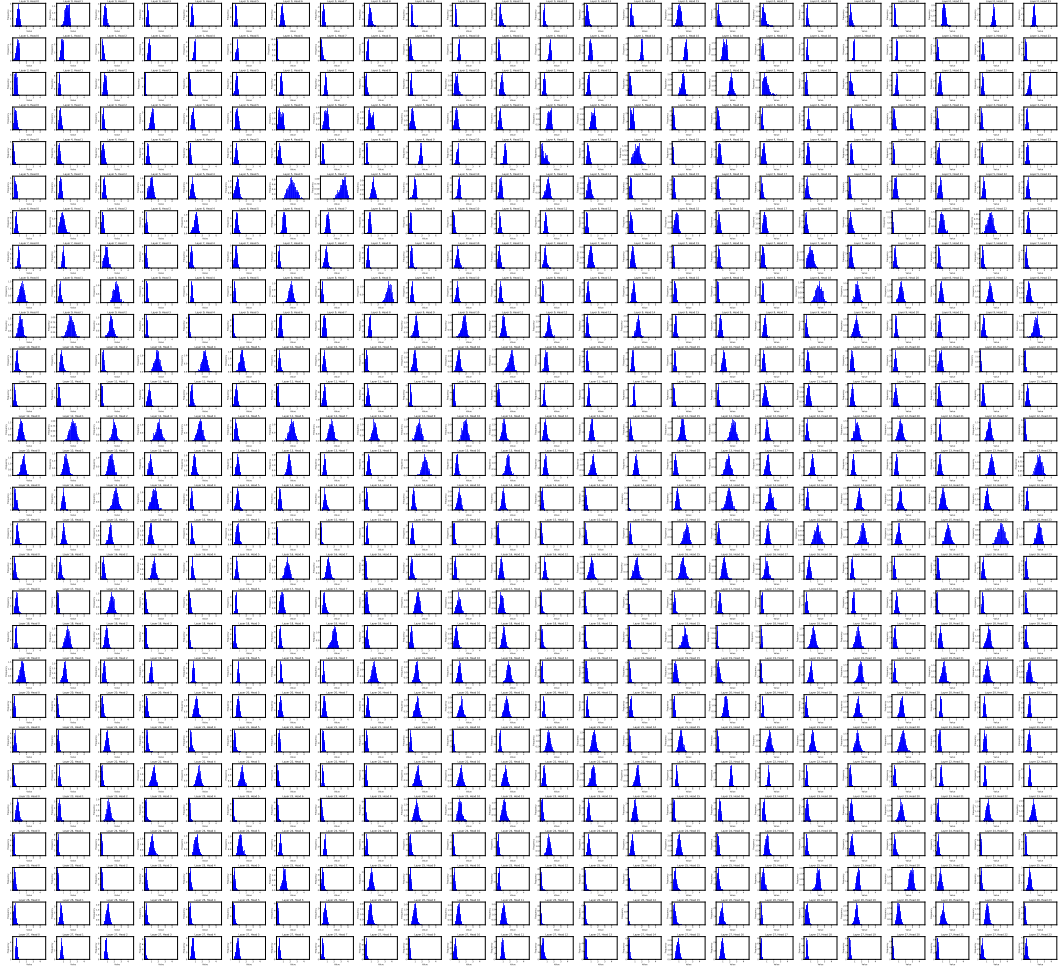


Figure 16: (see on screen) The distribution of RC upper bound (overlap area) for QmSum dataset. The first (last) row corresponds to heads in the first (last) layer.

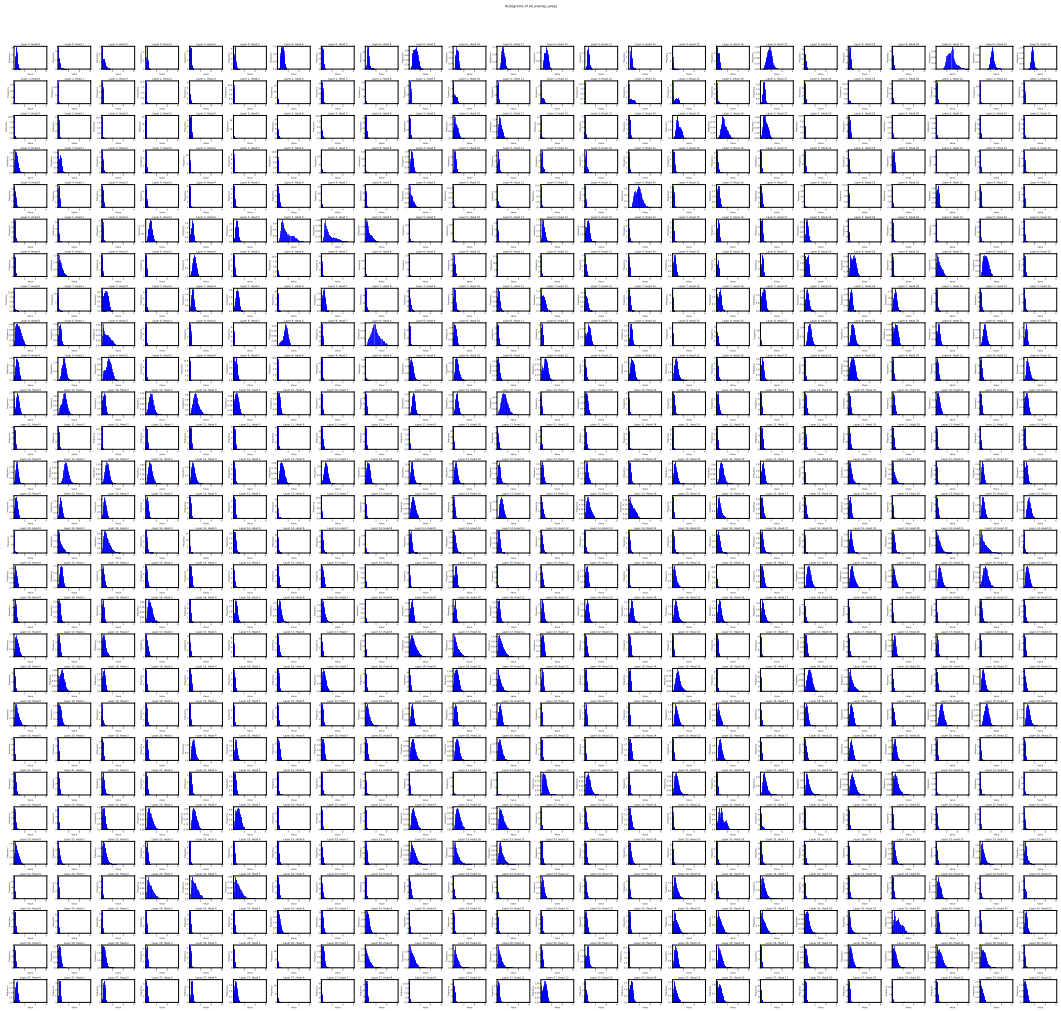


Figure 17: (see on screen) The distribution of RC upper bound (overlap area) for Squad v2 dataset. The first (last) row corresponds to heads in the first (last) layer.

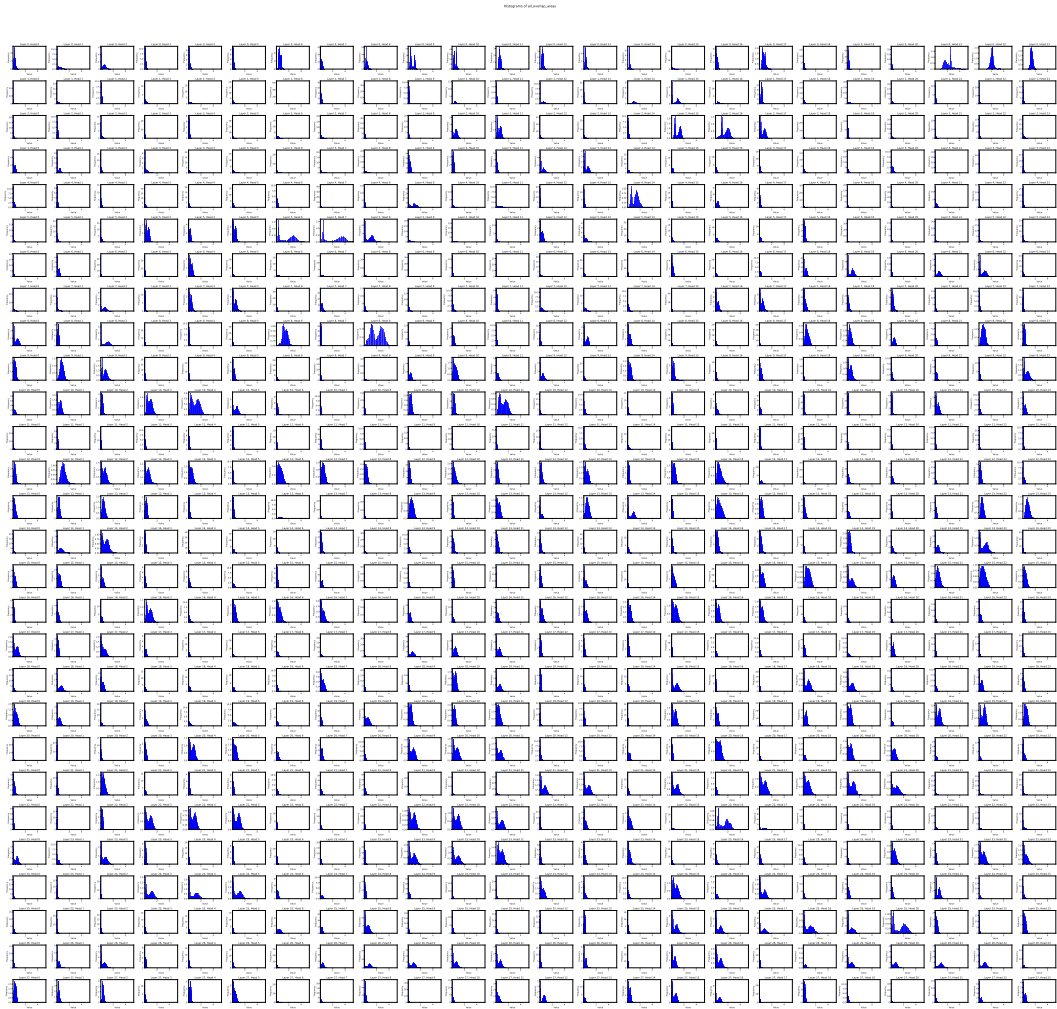


Figure 18: (see on screen) The distribution of RC upper bound (overlap area) for 2WikiMultiHop dataset. The first (last) row corresponds to heads in the first (last) layer.

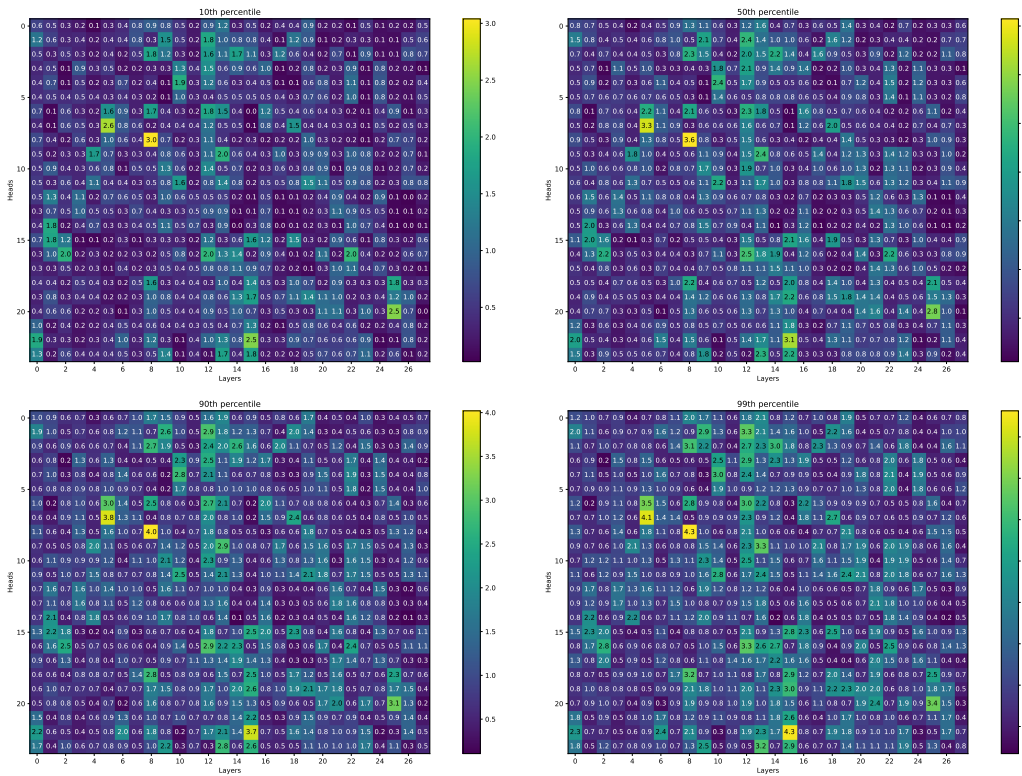


Figure 19: (see on screen) Percentiles of RC upper bound (overlap area) across the QmSum dataset

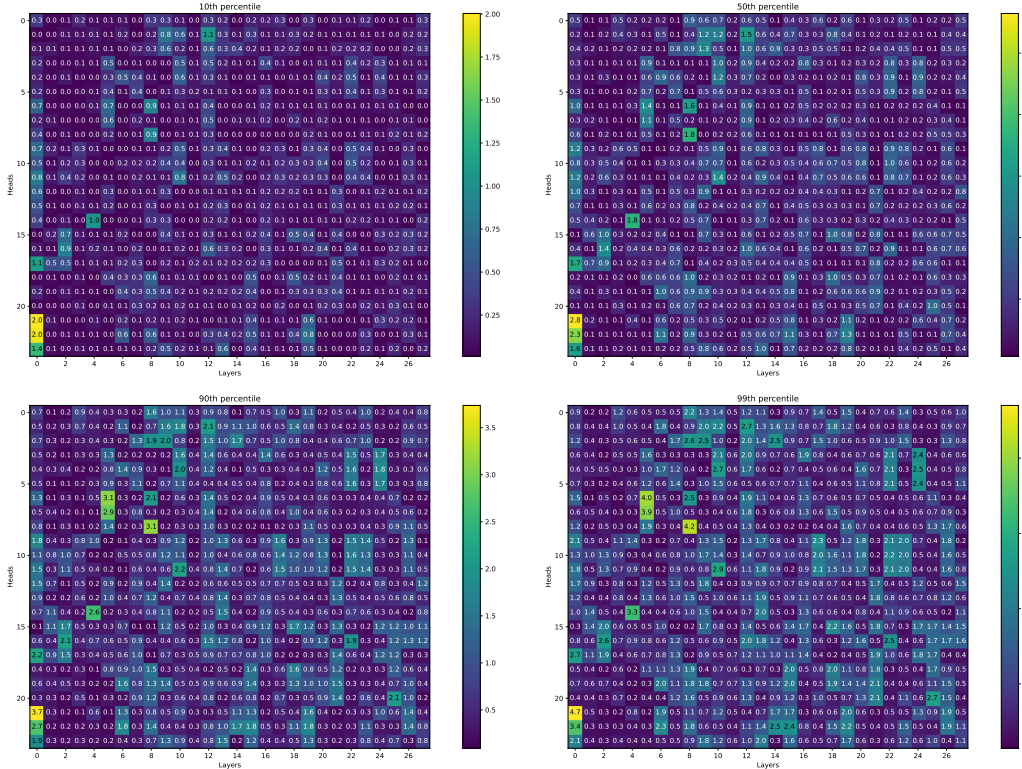


Figure 20: (see on screen) Percentiles of RC upper bound (overlap area) across the Squad dataset

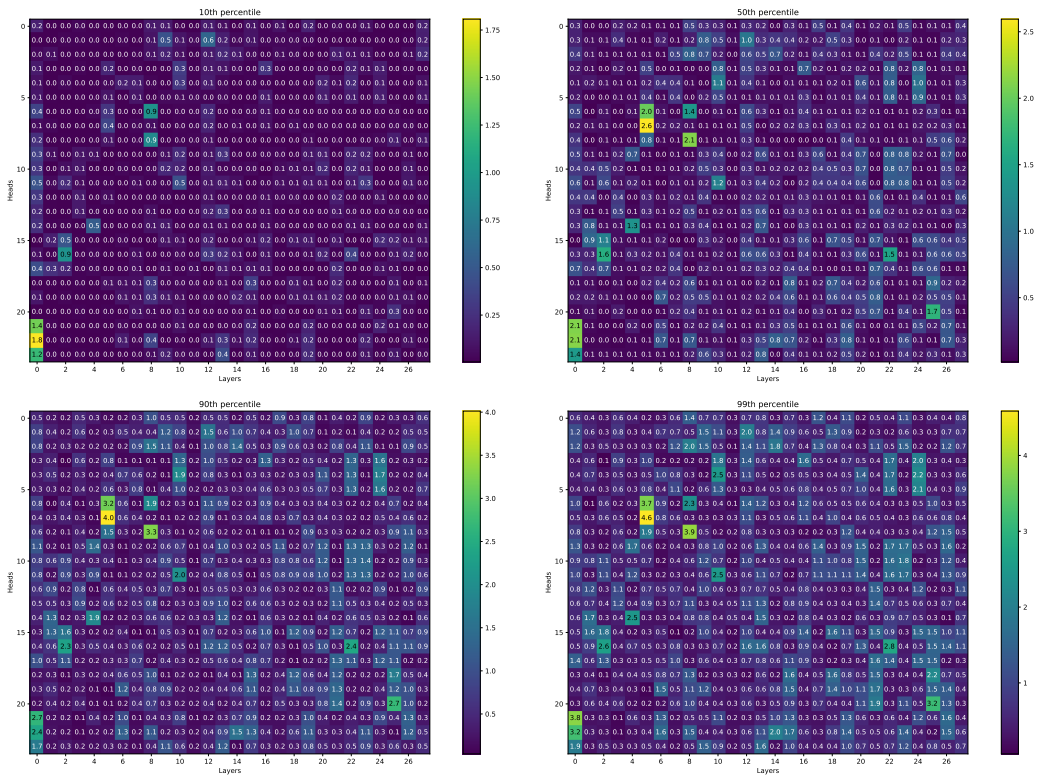


Figure 21: (see on screen) Percentiles of RC upper bound (overlap area) across the 2WikiMultiHop dataset

SALES SUMMARY REPORT

Location(s): Wax It Skin Studio
Period: November 1 - November 30, 2023

Date	# Sales	# Services	Service Sales	# Products	Product Sales	Net Total	Taxes	Tips	Gross Total
Nov 1	10	5	\$500.00	7	\$343.95	\$1,174.45	\$28.89	\$180.88	\$1,384.22
Nov 2	17	18	\$1,330.50	9	\$519.60	\$1,850.10	\$43.65	\$226.65	\$2,120.40
Nov 3	5	5	\$621.00	3	\$208.00	\$829.00	\$17.48	\$124.20	\$970.68
Nov 6	9	8	\$972.00	3	\$150.00	\$1,122.00	\$12.60	\$180.45	\$1,315.05
Nov 7	7	6	\$675.00	1	\$58.00	\$733.00	\$4.87	\$126.75	\$864.62
Nov 8	6	6	\$582.00	3	\$223.00	\$805.00	\$18.73	\$82.20	\$905.93
Nov 9	12	14	\$1,263.75	3	\$218.00	\$1,481.75	\$18.31	\$216.95	\$1,717.01
Nov 10	4	6	\$385.00	1	\$32.00	\$417.00	\$2.69	\$77.00	\$496.69
Nov 11	1	2	\$270.00	0	\$0.00	\$270.00	\$0.00	\$54.00	\$324.00
Nov 13	13	16	\$1,586.00	2	\$150.00	\$1,736.00	\$12.60	\$266.45	\$2,015.05
Nov 14	15	21	\$2,011.00	0	\$0.00	\$2,011.00	\$0.00	\$414.95	\$2,425.95
Nov 15	10	8	\$745.00	3	\$213.00	\$958.00	\$17.90	\$118.00	\$1,093.90
Nov 16	9	11	\$1,565.00	6	\$513.00	\$2,078.00	\$43.10	\$312.25	\$2,433.35
Nov 17	17	24	\$1,797.50	0	\$0.00	\$1,797.50	\$0.00	\$388.25	\$2,185.75
Nov 18	2	0	\$0.00	0	\$0.00	\$0.00	\$0.00	\$0.00	\$0.00
Nov 19	2	0	\$0.00	0	\$0.00	\$0.00	\$0.00	\$0.00	\$0.00
Nov 20	15	17	\$1,777.50	1	\$36.95	\$1,814.45	\$3.10	\$336.00	\$2,153.55
Nov 21	17	24	\$2,640.00	4	\$177.00	\$2,817.00	\$14.88	\$313.00	\$3,144.88
Nov 22	10	8	\$945.00	5	\$238.00	\$1,183.00	\$20.01	\$77.50	\$1,280.51
Nov 24	2	0	\$0.00	0	\$0.00	\$0.00	\$0.00	\$0.00	\$0.00

Page 1 of 2

SALES SUMMARY REPORT

Location(s): Wax It Skin Studio
Period: November 1 - November 30, 2023

Date	# Sales	# Services	Service Sales	# Products	Product Sales	Net Total	Taxes	Tips	Gross Total
Nov 1	10	5	\$500.00	7	\$343.95	\$1,174.45	\$28.89	\$180.88	\$1,384.22
Nov 2	17	18	\$1,330.50	9	\$519.60	\$1,850.10	\$43.65	\$226.65	\$2,120.40
Nov 3	5	5	\$621.00	3	\$208.00	\$829.00	\$17.48	\$124.20	\$970.68
Nov 6	9	8	\$972.00	3	\$150.00	\$1,122.00	\$12.60	\$180.45	\$1,315.05
Nov 7	7	6	\$675.00	1	\$58.00	\$733.00	\$4.87	\$126.75	\$864.62
Nov 8	6	6	\$582.00	3	\$223.00	\$805.00	\$18.73	\$82.20	\$905.93
Nov 9	12	14	\$1,263.75	3	\$218.00	\$1,481.75	\$18.31	\$216.95	\$1,717.01
Nov 10	4	6	\$385.00	1	\$32.00	\$417.00	\$2.69	\$77.00	\$496.69
Nov 11	1	2	\$270.00	0	\$0.00	\$270.00	\$0.00	\$54.00	\$324.00
Nov 13	13	16	\$1,586.00	2	\$150.00	\$1,736.00	\$12.60	\$266.45	\$2,015.05
Nov 14	15	21	\$2,011.00	0	\$0.00	\$2,011.00	\$0.00	\$414.95	\$2,425.95
Nov 15	10	8	\$745.00	3	\$213.00	\$958.00	\$17.90	\$118.00	\$1,093.90
Nov 16	9	11	\$1,565.00	6	\$513.00	\$2,078.00	\$43.10	\$312.25	\$2,433.35
Nov 17	17	24	\$1,797.50	0	\$0.00	\$1,797.50	\$0.00	\$388.25	\$2,185.75
Nov 18	2	0	\$0.00	0	\$0.00	\$0.00	\$0.00	\$0.00	\$0.00
Nov 19	2	0	\$0.00	0	\$0.00	\$0.00	\$0.00	\$0.00	\$0.00
Nov 20	15	17	\$1,777.50	1	\$36.95	\$1,814.45	\$3.10	\$336.00	\$2,153.55
Nov 21	17	24	\$2,640.00	4	\$177.00	\$2,817.00	\$14.88	\$313.00	\$3,144.88
Nov 22	10	8	\$945.00	5	\$238.00	\$1,183.00	\$20.01	\$77.50	\$1,280.51
Nov 24	2	0	\$0.00	0	\$0.00	\$0.00	\$0.00	\$0.00	\$0.00

Page 1 of 2

Date	# Sales	# Services	Service Sales	# Products	Product Sales	Net Total	Taxes	Tips	Gross Total
Nov 25	3	0	\$0.00	0	\$0.00	\$0.00	\$0.00	\$0.00	\$0.00
Nov 26	2	0	\$0.00	0	\$0.00	\$0.00	\$0.00	\$0.00	\$0.00
Nov 27	6	0	\$0.00	0	\$0.00	\$0.00	\$0.00	\$0.00	\$0.00
Nov 28	16	19	\$2,565.00	2	\$123.00	\$2,708.00	\$10.34	\$490.25	\$3,208.59
Nov 29	10	13	\$1,270.00	0	\$0.00	\$1,270.00	\$0.00	\$284.90	\$1,554.90
Nov 30	22	18	\$1,665.00	12	\$720.80	\$2,406.30	\$60.56	\$293.00	\$2,759.86
Total	242	252	\$25,537.25	65	\$3,924.38	\$29,461.55	\$329.71	\$4,563.23	\$34,354.49

* The service sales include the value of applied packages.

Date	# Sales	# Services	Service Sales	# Products	Product Sales	Net Total	Taxes	Tips	Gross Total
Nov 25	3	0	\$0.00	0	\$0.00	\$0.00	\$0.00	\$0.00	\$0.00
Nov 26	2	0	\$0.00	0	\$0.00	\$0.00	\$0.00	\$0.00	\$0.00
Nov 27	6	0	\$0.00	0	\$0.00	\$0.00	\$0.00	\$0.00	\$0.00
Nov 28	16	19	\$2,565.00	2	\$123.00	\$2,708.00	\$10.34	\$490.25	\$3,208.59
Nov 29	10	13	\$1,270.00	0	\$0.00	\$1,270.00	\$0.00	\$284.90	\$1,554.90
Nov 30	22	18	\$1,665.00	12	\$720.80	\$2,406.30	\$60.56	\$293.00	\$2,759.86
Total	242	252	\$25,537.25	65	\$3,924.38	\$29,461.55	\$329.71	\$4,563.23	\$34,354.49

* The service sales include the value of applied packages.

(a) Top-scoring head (Head 30)

(b) Mean of all heads

SALES SUMMARY REPORT

Location(s): Wax It Skin Studio
Period: November 1 - November 30, 2023

Date	# Sales	# Services	Service Sales	# Products	Product Sales	Net Total	Taxes	Tips	Gross Total
Nov 1	10	8	\$830.50	7	\$343.95	\$1,174.45	\$28.89	\$180.88	\$1,384.22
Nov 2	17	18	\$1,330.50	9	\$519.60	\$1,850.10	\$43.65	\$226.65	\$2,120.40
Nov 3	5	5	\$621.00	3	\$208.00	\$829.00	\$17.48	\$124.20	\$970.68
Nov 6	9	8	\$972.00	3	\$150.00	\$1,122.00	\$12.60	\$180.45	\$1,315.05
Nov 7	7	6	\$675.00	1	\$58.00	\$733.00	\$4.87	\$126.75	\$864.62
Nov 8	6	6	\$582.00	3	\$223.00	\$805.00	\$18.73	\$82.20	\$905.93
Nov 9	12	14	\$1,263.75	3	\$218.00	\$1,481.75	\$18.31	\$216.95	\$1,717.01
Nov 10	4	6	\$385.00	1	\$32.00	\$417.00	\$2.69	\$77.00	\$496.69
Nov 11	1	2	\$270.00	0	\$0.00	\$270.00	\$0.00	\$54.00	\$324.00
Nov 13	13	16	\$1,586.00	2	\$150.00	\$1,736.00	\$12.60	\$266.45	\$2,015.05
Nov 14	15	21	\$2,011.00	0	\$0.00	\$2,011.00	\$0.00	\$414.95	\$2,425.95
Nov 15	10	8	\$745.00	3	\$213.00	\$958.00	\$17.90	\$118.00	\$1,093.90
Nov 16	9	11	\$1,565.00	6	\$513.00	\$2,078.00	\$43.10	\$312.25	\$2,433.35
Nov 17	17	24	\$1,797.50	0	\$0.00	\$1,797.50	\$0.00	\$388.25	\$2,185.75
Nov 18	2	0	\$0.00	0	\$0.00	\$0.00	\$0.00	\$0.00	\$0.00
Nov 19	2	0	\$0.00	0	\$0.00	\$0.00	\$0.00	\$0.00	\$0.00
Nov 20	15	17	\$1,777.50	1	\$36.95	\$1,814.45	\$3.10	\$336.00	\$2,153.55
Nov 21	17	24	\$2,640.00	4	\$177.00	\$2,817.00	\$14.88	\$313.00	\$3,144.88
Nov 22	10	8	\$945.00	5	\$238.00	\$1,183.00	\$20.01	\$77.50	\$1,280.51
Nov 24	2	0	\$0.00	0	\$0.00	\$0.00	\$0.00	\$0.00	\$0.00

Page 1 of 2

Date	# Sales	# Services	Service Sales	# Products	Product Sales	Net Total	Taxes	Tips	Gross Total
Nov 25	3	0	\$0.00	0	\$0.00	\$0.00	\$0.00	\$0.00	\$0.00
Nov 26	2	0	\$0.00	0	\$0.00	\$0.00	\$0.00	\$0.00	\$0.00
Nov 27	6	0	\$0.00	0	\$0.00	\$0.00	\$0.00	\$0.00	\$0.00
Nov 28	16	19	\$2,565.00	2	\$123.00	\$2,708.00	\$10.34	\$490.25	\$3,208.59
Nov 29	10	13	\$1,270.00	0	\$0.00	\$1,270.00	\$0.00	\$284.90	\$1,554.90
Nov 30	22	18	\$1,665.00	12	\$720.80	\$2,406.30	\$60.56	\$293.00	\$2,759.86
Total	242	252	\$25,537.25	65	\$3,924.38	\$29,461.55	\$329.71	\$4,563.23	\$34,354.49

* The service sales include the value of applied packages.

(c) Worst-scoring head (Head 16)

Figure 22: Attention heatmaps from Layer 15 using three attribution strategies. The top head yields focused and accurate attribution, the mean head shows diluted but somewhat relevant attention, and the worst head highlights largely irrelevant regions.